Available online at www.sciencedirect.com

ScienceDirect

Geochimica et Cosmochimica Acta 232 (2018) 82–100

Geochimica et Cosmochimica Acta

www.elsevier.com/locate/gca

Evolution of atmospheric xenon and other noble gases inferred from Archean to Paleoproterozoic rocks

G. Avice [a,*], B. Marty [a], R. Burgess [b], A. Hofmann [c], P. Philippot [d,e], K. Zahnle [f], D. Zakharov [g]

[a] *Centre de Recherches Pétrographiques et Géochimiques, CRPG-CNRS, Université de Lorraine, UMR 7358, 15 rue Notre Dame des Pauvres, BP 20, 54501 Vandoeuvre-lès-Nancy, France*

[b] *School of Earth and Environmental Sciences, University of Manchester, Oxford Road, Manchester M13 9PL, UK*

[c] *Department of Geology, University of Johannesburg, P.O. Box 524, Auckland Park 2006, South Africa*

[d] *Institut de Physique du Globe de Paris, Université Sorbonne Paris Cité, UMR 7154, Paris F-75238, France*

[e] *Géosciences Montpellier, Université de Montpellier, UMR 5243 CNRS, Place Eugène Bataillon, 34095 Montpellier, France*

[f] *NASA Ames Research Center, Moffett Field, CA 94035, USA*

[g] *Department of Earth Sciences, University of Oregon, Eugene, OR 97403, USA*

Received 15 November 2017; accepted in revised form 16 April 2018; available online 26 April 2018

Abstract

We have analyzed ancient atmospheric gases trapped in fluid inclusions contained in minerals of Archean (3.3 Ga) to Paleozoic (404 Ma) rocks in an attempt to document the evolution of the elemental composition and isotopic signature of the atmosphere with time. Doing so, we aimed at understanding how physical and chemical processes acted over geological time to shape the modern atmosphere.

Modern atmospheric xenon is enriched in heavy isotopes by 30–40‰ u^{-1} relative to Solar or Chondritic xenon. Previous studies demonstrated that, 3.3 Ga ago, atmospheric xenon was isotopically fractionated (enriched in the light isotopes) relative to the modern atmosphere, by 12.9 ± 1.2 (1σ) ‰ u^{-1}, whereas krypton was isotopically identical to modern atmospheric Kr. Details about the specific and progressive isotopic fractionation of Xe during the Archean, originally proposed by Pujol et al. (2011), are now well established by this work. Xe isotope fractionation has evolved from 21‰ u^{-1} at 3.5 Ga to 12.9‰ u^{-1} at 3.3 Ga. The current dataset provides some evidence for stabilization of the Xe fractionation between 3.3 and 2.7 Ga. However, further studies will be needed to confirm this observation. After 2.7 Ga, the composition kept evolving and reach the modern-like atmospheric Xe composition at around 2.1 Ga ago.

Xenon may be the second atmospheric element, after sulfur, to show a secular isotope evolution during the Archean that ended shortly after the Archean-Proterozoic transition. Fractionation of xenon indicates that xenon escaped from Earth, probably as an ion, and that Xe escape stopped when the atmosphere became oxygen-rich. We speculate that the Xe escape was enabled by a vigorous hydrogen escape on the early anoxic Earth. Organic hazes, scavenging isotopically heavy Xe, could also have played a role in the evolution of atmospheric Xe.

For 3.3 Ga-old samples, Ar-N_2 correlations are consistent with a partial pressure of nitrogen (pN_2) in the Archean atmosphere similar to, or lower than, the modern one, thus requiring other processes than a high pN_2 to keep the Earth's surface

* Corresponding author at: California Institute of Technology, Department of Geological and Planetary Sciences, MC170-25, 1200 East California Boulevard, Pasadena, CA 91125, USA.

E-mail addresses: gavice@caltech.edu, avice.guillaume@gmail.com (G. Avice).

https://doi.org/10.1016/j.gca.2018.04.018

warm despite a fainter Sun. The nitrogen isotope composition of the atmosphere at 3.3 Ga was already modern-like, attesting to inefficient nitrogen escape to space since that time.

Keywords: Noble gases; Xenon; Archean; Atmosphere; Escape

1. INTRODUCTION

The origin of the volatile elements in the Earth's atmosphere and mechanisms responsible for its subsequent evolution remain poorly understood (Marty, 2012). The elemental and isotopic composition of the Earth's atmosphere has been shaped by numerous events in the history of our planet including contributions from diverse extraterrestrial sources during the accretion, meteoritic and cometary impacts, mantle degassing, subduction with crustal recycling of volatile-rich lithologies and atmospheric escape. Despite the presence of a geological rock record, little is known about the state of the atmosphere during the Archean (4.0–2.5 Ga), an epoch covering one third of Earth's history and during which early forms of life emerged and evolved (Nisbet and Sleep, 2001). Some isotopic signatures in ancient sediments point to major differences in the composition of the atmosphere in the Archean and early Paleoproterozoic eons. For example, sulfur isotopes measured in rocks older than ≈2.3 Ga carry a mass-independent fractionation (MIF) signature originating from photochemical reactions involving UV photons in a O_2-poor atmosphere (Farquhar and Wing, 2003; Catling, 2014). Furthermore, an atmospheric composition very different from the modern one seems to be required to maintain a warm temperature (liquid water) at the Earth's surface despite a reduced solar luminosity in the past (Schwarzschild, 1958), the so-called "faint young sun paradox" (Ulrich, 1975).

Noble gases are chemically inert elements that are powerful tracers of the formation and subsequent evolution of the Earth's atmosphere. Xenon (Xe), the heaviest stable noble gas, has nine isotopes that present mass-dependent isotope variations. Some Xe isotopes have also been contributed by extinct (^{129}I, $T_{1/2}$ = 15.7 Ma; ^{244}Pu; $T_{1/2}$ = 82 Ma) and extant (^{238}U; $T_{1/2}$ = 4.47 Ga) radioactive nuclides. Terrestrial atmospheric Xe has two unique features. First, atmospheric Xe is depleted by a factor of 20 compared to the Ar/Kr/Xe elemental pattern defined by chondrites (e.g., Pepin (1991)). Second, atmospheric xenon is strongly enriched in heavy relative to light isotopes with a mass-dependent fractionation of 30–40‰ u^{-1} (computed from light isotopes which are devoid of radioactive nuclide contribution) compared to other known solar system components such as AVCC-Xe (Average Carbonaceous Chondrite Xe) or SW-Xe (Solar Wind Xe) (Ott, 2014). These two features form the "xenon paradox" (Ozima and Podosek, 2002).

An additional striking feature of atmospheric Xe is that it cannot be directly related to either chondritic Xe or solar Xe. When corrected for mass-dependent isotope fractionation, the heavy Xe isotopes ^{134}Xe and ^{136}Xe are depleted relative to both Solar and Chondritic signatures (Pepin, 1991). This is a problematic issue since no known nuclear process can selectively decrease the abundance of these isotopes in the atmosphere. Furthermore, spontaneous fission of extinct ^{244}Pu ($T_{1/2}$ = 82 Ma) and extant ^{238}U ($T_{1/2}$ = 4.47 Ga), which produce the heavy isotopes of Xe in the silicate Earth, would have increased levels of ^{134}Xe and ^{136}Xe in the atmosphere with time due to mantle and crustal degassing, making the imbalance even more severe. An alternative and mathematically-derived initial Xe component, labeled U-Xe, has thus been defined in previous studies (Takaoka, 1972; Pepin, 1991) and is considered as the starting isotopic composition for the Earth's atmosphere. Recent results obtained on 3.3 Ga-old samples from the Barberton Greenstone Belt (South Africa) demonstrated the existence of the U-Xe early in Earth's history (Avice et al., 2017). Finally, after decades of unsuccessful searching for this component, recent measurements of the isotopic composition of Xe in the coma of comet 67P/Churyumov-Gerasimenko revealed that the progenitor of atmospheric Xe, the U-Xe, reflects a mix between about 22% of cometary Xe (strongly depleted in ^{134}Xe and ^{136}Xe) and 78% chondritic Xe (Marty et al., 2017).

Even assuming U-Xe as the starting isotopic composition for the atmosphere, solving the xenon paradox calls for complex models with episodes of mantle degassing and early isotopic fractionation of atmospheric noble gases driven by hydrodynamic escape of hydrogen (Pepin, 1991), and/or late addition of cometary gases to a residual, fractionated atmosphere (Dauphas, 2003). In these models, Xe processing and fractionation occurred during the earliest stages of terrestrial accretion (see a review by Dauphas and Morbidelli, 2014). Some recent studies call these models into question and propose instead that the depletion and isotopic fractionation of Xe took place progressively during geological eons. This model is based on the analysis of xenon in ancient rocks (Srinivasan, 1976; Pujol et al., 2009; Pujol et al., 2011; Avice et al., 2017; Bekaert et al., 2018) or in ancient fluids (Holland et al., 2013; Warr et al., 2018) that reveal a stable isotope composition of xenon intermediate between those of the potential cosmochemical ancestors and of the modern atmosphere. Pujol et al. (2011) proposed that the isotope fractionation of atmospheric xenon was a long-term process that was still active during the Archean eon. This fractionation has to be specific to Xe, since other noble gases do not appear to have been fractionated. Because xenon is the heaviest noble gas, only non-thermal escape of this element would have been possible, perhaps related to its specific electronic structure, which makes it more prone to ionization by solar UV photons than other noble gases. These results have thus been subsequently interpreted as an evidence for a continuous

atmospheric escape of Xe during the Archean accompanied by an instantaneous isotopic fractionation (Marrocchi et al. 2011; Kuga et al. 2015) when Xe is ionized in the presence of organic molecules (Marty, 2012; Hébrard and Marty, 2014). Hébrard and Marty (2014) built a 1D photochemical model of the Archean atmosphere proposing that the enhanced EUV flux from the young Sun (Ribas et al., 2005) ionized Xe atoms preferentially at altitudes between 90 and 110 km. This altitude range coincided with the maximum production of organic haze from photochemistry of H_2 - CH_4 mixtures (two species often advocated to have been present in the Archean atmosphere). Independently, laboratory experiments involving Xe ions trapped in forming organic matter (Frick et al., 1977; Marrocchi et al., 2011; Kuga et al., 2015; Kuga et al., 2017) have shown a Xe mass-dependent instantaneous fractionation factor (α) of $10 \pm 4‰\ u^{-1}$ in favor of the heavy isotopes. This α value is within the range of those needed to yield an integrated fractionation of 30–40‰ u^{-1} for a Xe depletion of a factor of 20 in a leaking atmosphere, assuming a Rayleigh-type distillation during escape (Marty, 2012). Therefore, Hébrard and Marty (2014) concluded that xenon in the Archean atmosphere was partly trapped and isotopically fractionated in organic haze, while other Xe ions were escaping to space. An alternative model is that mass fractionation is generated directly by the hydrodynamic escape of Xe ions (Zahnle, 2018).

Even if previous studies provided a framework for understanding the xenon paradox described above, there are still some unresolved issues. (i) The above view is based on the analysis of a limited number of samples including: two barite samples from the 3.5 Ga-old Dresser Formation, Pilbara craton, Australia, (Srinivasan,1976; Pujol et al., 2009); fluid inclusions in quartz, also from the Dresser Formation (Pujol et al., 2011)); and 3.3 Ga-old samples from the Barberton Greenstone Belt, South Africa (Avice et al., 2017). (ii) The atmospheric origin of trapped Xe in these samples has been questioned by Pepin (2013) who suggested that Xe trapped in these samples is a mixture between modern-like atmospheric Xe and mantle Xe, although the arguments on which this was based have been contested by Pujol et al. (2013b). (iii) If the concept of Xe isotope fractionation described above is correct, the physical processes behind the escape of Xe atoms and/or ions are still unknown and additional measurements are thus needed to understand these phenomena. (iv) The similarity in isotopic composition of atmospheric Xe on Mars and on Earth is a major issue for the "haze-Xe" model (Hébrard and Marty, 2014), because there is no evidence for the existence of such haze production in the early Martian atmosphere, although it cannot be excluded as the presence of CH_4 in the modern Martian atmosphere has been reported (Formisano et al., 2004)). (v) Finally, the exact timing and mode of the evolution of the isotopic composition of atmospheric Xe is ill-defined. Thus far, it is difficult to link this evolution to other geochemical cycles, such as the progressive oxidation of the atmosphere for example. In order to document these issues, we present new high-precision analyses of Xe contained in fluid inclusions in quartz of different ages (3.3 Ga–404 Ma) and from different geological settings (Table 1) and demonstrate an evolution of the isotopic composition of atmospheric Xe during several billion years. In addition, a comprehensive study of noble gases (Ne, Ar, Kr, Xe) and nitrogen in 3.3 Ga-old samples from the Barberton area also enables the isotopic composition of the atmosphere at that time to be defined at high precision.

2. SAMPLES AND ANALYTICAL METHODS

Brief descriptions of the analyzed samples, their geological age constraints and of the analytical methods are presented in this section.

2.1. Geological setting of the samples and age constraints

Samples analyzed in this study consist of high-purity macro-crystalline quartz crystals containing numerous fluid inclusions, except for samples of meta-carbonates from Isua (Greenland) that consist of a mixture of carbonate and quartz crystals. The high proportion of fluid inclusions ensured that the quantities of gas released during crushing experiments were sufficient to determine Xe isotopic ratios at high precision and that impurities did not pollute the Xe signal (for example by neutron capture on Ba or Te nuclide producing Xe isotopes; Pujol et al., 2009). Localities of the analyzed samples are summarized in Table 1.

Samples from the Barberton greenstone belt were recovered from quartz veins cutting across cores recovered during an ICDP drilling project (Arndt et al., 2012) and are described in more details by Avice et al. (2017). Ar-Ar dating gave an age of 3.30 ± 0.05 (1σ) Ga in agreement with the age of the main deformation event "D_2" defined for this geological area that led to regional-scale fluid circulation (de Ronde and Wit, 1994).

Samples from the Boongal and Maddina formations (Fortescue Group, Hamersley Basin, Australia) are from quartz precipitates in pillow-basalts. Comparable quartz pods in the 3.49 Ga-old North Pole area had already been considered as being derived from early hydrothermal circulations after lava eruption (Foriel et al., 2004). Ar-Ar dating did not constrain the age of these samples because of (i) too low abundances of potassium and (ii) ^{40}Ar excess uncorrelated with the chlorine content as usually seen in other studies (Kendrick et al., 2001). A maximum age of 2.74 Ga is thus inferred from U-Pb dating of the host rocks (Trendall et al., 2004).

Supracrustal rocks from the Isua greenstone belt (West Greenland) are thought to be up to 3.8 Ga-old (Nutman and Friend, 2009). Samples analyzed in this study were collected in the southern part of the belt and consisted of quartz crystals mixed with carbonates probably of metasomatic origin (Rose et al., 1996). An Eoarchean age for the quartz is thus doubtful and the widespread resetting event at 2.3 ± 0.2 Ga identified by Sm-Nd dating on metamorphic garnets from the same area (Blichert-Toft and Frei, 2001) might be a more probable age for fluid trapping in these samples (see Results and Implications sections for details on the choice of the age).

Quartz samples from the Quetico Belt are from veins cutting across meta-greywackes dated at ca. 2.7 Ga (Davis

Table 1
Locations, types and ages of samples analyzed in this study. The isotopic fractionations of Xe relative to modern air (δXe_{air}) and to U-Xe ($\delta Xe_{U\text{-}Xe}$) are indicated together with Xe isotopes used to compute these fractionation factors (see text). The corresponding remaining atmospheric fractionations and depletion factors for the Rayleigh's distillation model (see text) are also indicated. Results from previous studies are also listed (Srinivasan, 1976; Meshik et al., 2001; Pujol et al., 2009; Pujol et al., 2011; Holland et al., 2013; Pujol et al., 2013a,b). Errors at 1σ.

Sample locality	Lithology	Age (Ga)	±	δXe_{air} (‰.u^{-1})	±	MSWD	Xe isotopes (/^{130}Xe) used to compute the fractionation	$\delta Xe_{U\text{-}Xe}$ (‰ u^{-1})	±	Remaining fraction	±	Depletion	±	Reference
Previous studies														
North Pole (Australia)	Barite	3.48	0.09	21	3	n.d.	129,132,136	17	2	0.24	+0.05/ −0.04	4.2	+0.9/ −0.8	Pujol et al. (2009)
North Pole (Australia)	Barite	3.5	n.d.	13.7	n.d.	n.d.	134,136							Srinivasan (1976)
North Pole (Australia)	Quartz	3.1	0.4	15	5	n.d.	128,129,132,134,136							Pujol et al. (2013)
North Pole (Australia)	Quartz	3.0	+0.2	10	5	n.d.	128,129,131							Pujol et al. (2011)
Timmins (Canada)	Fluid	See text	–	3	1	0.067	124,126,128,130	–	–					Holland et al. (2013)
Belorechenskoe (Russia)	Barite	0.170	0.015	0.5	n.d.	n.d.	124,126,128,129	–	–					Meshik et al. (2001)
This study														
Barberton (South Africa)	Quartz	3.3	0.05	12.9	1.2	1.4	126,128,130,131	25	1	0.11	0.01	8.2	0.7	This study
Fortescue (Australia)	–	2.7	n.d.	13.0	1.2	0.9	126,128,130,131	25	1	0.11	0.01	8.2	0.7	–
Quetico Belt (Canada)	–	2.55	0.15	3.8	2.5	0.42	124,126,128,129,130,131	35	2	0.05	0.01	19	+4/ −3	–
Vetreny Belt (Russia)	–	2.45	n.d.	6.6	1.5	0.8	124,126,128,129,130,131	29.2	1.35	0.08	0.01	11	+1/ −1	–
Isua (Greenland)	–	2.3	0.3	5.8	1.5	0.3	124,126,128,129,130,131	30.5	1.4	0.07	0.01	13.2	+1.7/ −1.5	–
Carnaiba (Brasil)	–	2.0	0.1	1.8	2.2	1.12	124,126,128,129,130,131	34	4	0.05	0.02	17	+7/ −5	–
Gaoua (Burkina Faso)	–	2.10	0.07	2.6	2.1	0.94	124,126,128,129,131	36	2	0.05	0.01	21	+4/ −3	–
Caramal (Australia)	–	1.7	??	0.32	0.78	0.89	124–136	–	–					–
Avranches (France)	–	0.53	0.01	1.5	1.6	0.12	124–136	–	–					–
Rhynie (Scotland)	–	0.404	0.001	0.1	1.9	0.28	124–136	–	–					–

et al., 1990). The true age of the veins is unknown, but it is likely close to 2.65 Ga, the age of regional metamorphism and the onset of late granitoid plutonism (Card, 1990).

The Vetreny Belt samples were collected from quartz-epidote veins that dissect hydrothermally altered komatiitic basalts. Based on field observations, the Vetreny Belt is regarded as a rift that formed in a submarine environment as part of a paleoproterozoic large igneous province on the Baltic Shield (Kulikov et al., 2010). Ubiquitous quartz-epidote veins represent hydrothermal fluid precipitates, which formed during reaction between cooling basalts and contemporaneous oceanic water (Zakharov and Bindeman, 2015). These rocks have been dated using Sm-Nd and Re-Os isochrons, bracketing the age of the komatiitic basalts between 2.43 and 2.41 Ga (Puchtel et al., 2016; Mezhelovskaya et al., 2016). Dacites that represent the earliest rocks erupted in the Vetreny Belt rift gave a U-Pb zircon age of 2437 ± 4 Ma (Puchtel et al., 1997), which can be regarded as the maximum age of the Vetreny Belt rift.

Quartz samples located in veins from the Gaoua mine district (Burkina Faso) are linked to the early stages of formation of a porphyry deposit (Baratoux et al., 2015). Pyrite present in the quartz-bearing veins yielded a Re-Os age of 2.10 ± 0.07 Ga (1σ) (Le Mignot et al., 2014).

Samples from Carnaíba (Brazil) are quartz crystals from emerald-hosting veins linked to the intrusion of leucogranites in Proterozoic volcano-sedimentary sequences (Giuliani et al., 1990). The age of the mineralization is bracketed between 1.98 Ga and 1.93 Ga based on Ar-Ar dating of associated phlogopites (Cheilletz et al., 1993).

Samples from Caramal (Australia) are from quartz breccia zones located in the 1.8–1.7 Ga-old Kombolgie sandstones. Quartz is interpreted to have formed shortly after the crystallization of associated illite, which was dated at 1.6–1.7 Ga using the Ar-Ar method (Kyser et al., 2000 and refs. therein).

The sample from Avranches (France) is from quartz veins that cut across the western part of the Mancellian batholith. This area underwent several orogenic episodes but U-Pb dating on zircons reveals an age of 540 ± 10 Ma (1σ) for rocks from this region (Chantraine et al., 1994 and refs. therein).

The sample from Rhynie (NE Scotland) is a cherty (microcrystalline quartz) sample that has previously been shown to contain trapped paleo-atmospheric argon (Rice et al., 1995 and refs. therein) with a $^{40}Ar/^{36}Ar$ ratio of 289.5 ± 0.4 (1σ) (Stuart et al., 2016) and has an age of 403.9 ± 2.1 Ma (1σ) as reported by Mark et al. (2011), based on Ar-Ar plateau ages from K-feldspar-quartz veins.

Recent samples from Colombia (35 Ma; Giuliani et al., 2000), La Gardette mine (18–19 Ma, Mt Blanc, courtesy M. -C. Boiron) and from the Rhine Graben (ca. 30 Ma, courtesy M. -C. Boiron) were used to check the extraction, purification and measurement procedures.

2.2. Analytical methods

For Xe-Kr measurements (except for samples from the Vetreny Belt), gases were extracted from fluid inclusions contained in 2–3 mm-sized grains by crushing with a modified VAT® valve (Zimmermann, 2014). The bellow was replaced by a cylinder that crushes grains (up to 1 g) placed on a stainless steel disc, while the valve was progressively closed. Online Ti-sponge getters ensured the removal of reactive gases especially water, the major constituent of the fluid inclusions. Xenon was condensed on the walls of a glass tube immersed in liquid N_2 (77 K) for 20 min. Part of the krypton also condensed on this tube. After closing the valve between the glass tube and the purification line, the remaining fraction in the line containing Ar and light noble gases was pumped out for 10 min. While Xe and Kr were trapped on the walls of the glass tube, the glass tube also contained an appreciable Ar content in gaseous form that could potentially interfere with isotopic measurements. The Ar content was reduced by expanding the gas into the extraction line under static vacuum, followed by pumping after closing the valve to the glass finger. It was necessary to repeat this procedure up to 10 times to decrease the partial pressure of Ar (mainly ^{40}Ar present in fluid inclusions) before introducing the Xe-Kr gas fraction in the mass spectrometer. The Xe isotopic analyses were carried-out on a Thermofisher® Helix MC Plus noble gas mass spectrometer operated in peak jumping mode for abundances and Xe isotopic ratios measurements. The high stability of the mass spectrometer ensured a very good reproducibility of the standards measured during crushing experiments and enabled high precision data from samples. Xenon blanks were typically around 10^{-18} mol of ^{130}Xe and thus had a negligible contribution (usually <1%) on the Xe abundance measured during crushing (10^{-16}–10^{-15} mol ^{130}Xe). Krypton blanks were also negligible. All isotopic ratios presented in the Results section are corrected for blank contribution and mass discrimination of the mass spectrometer. A full propagation of the errors on the internal precision, the sensitivity of the mass spectrometer, the reproducibility of the standards and the blank contribution has been applied in order to take into account all potential sources of variability (*e.g.* Bekaert et al., 2017). The mass spectrometer sensitivity and mass discrimination were determined with known amounts of atmospheric noble gases following the same procedure as reported by Marty and Zimmermann (1999) and using the atmospheric compositions of Kr and Xe of Basford et al. (1973). Recent quartz samples (0–35 Ma) were analyzed using the same analytical procedures to check that there was no isotopic fractionation introduced by experimental artefacts. Except for some fissiogenic $^{131\text{-}136}Xe$ excesses, isotopic spectra of Xe released from recent quartz samples do not show any resolvable isotopic fractionation relative to the isotopic composition of the modern atmosphere with a maximum isotopic fractionation of 1.4 ± 1.6‰ u^{-1} (1σ).

Xenon and Kr from samples from the Vetreny belt (2.45 Ga) were extracted following a stepwise heating technique in an all-metal induction furnace (Zimmermann et al., 2017). Samples were dropped in a Ta crucible surrounded by an inductive coil. Temperature steps were 800 °C and 1700 °C followed by a re-extraction at 1700 °C. Noble gases were subsequently purified and analyzed following the method described above. Experimental procedures for the N_2-Ar-Ne determinations on different splits of a sample

from Barberton quartz (BMGA3-9) are given in the Supplementary Material.

3. RESULTS

3.1. Xenon and the Isotopic Fractionation of Ancient Atmospheres

Results for Xe isotopic ratios and abundances released during each extraction step are presented in Table S1 (Supplementary Material). The error-weighted mean for each isotopic ratio and the corresponding Mean Standard Weighted Deviation (MSWD) appear in bold. MSWD values are usually close to, or lower than 1, suggesting that sometimes errors may have been overestimated. Mean values of $^{131\text{-}136}Xe/^{130}Xe$ ratios were not computed for samples presenting important fissiogenic excesses. Mean isotopic ratios of Xe in Barberton quartz (Avice et al., 2017) are reproduced in Table S1 (Supplementary Material).

Isotopic spectra normalized to the isotopic composition of the modern atmosphere for xenon in Barberton, Fortescue Group, Vetreny Belt, Isua and Gaoua samples are shown in Fig. 1a–e. Isotopic spectra, without $^{132\text{-}136}Xe/^{130}Xe$ ratios affected by fissiogenic excesses, for Quetico Belt (2.7–2.65 Ga) and Carnaíba (2.1 Ga) samples are displayed in Fig. S1 and S2 (Supplementary Material), respectively.

For each spectrum in Fig. 1, light isotopes ($^{124\text{-}129}Xe$) released from fluid inclusions are enriched relative to the isotopic composition of the modern atmosphere, except for the Gaoua spectrum (2.1 Ga, Fig. 1e) where only some ^{128}Xe excess is definitely present and where $^{124}Xe/^{130}Xe$ and $^{126}Xe/^{130}Xe$ ratios, although imprecise, are higher than the atmospheric values. For Barberton (Fig. 1a) and Fortescue Group (Fig. 1b) samples, heavy isotopes ($^{131\text{-}136}Xe$) are also depleted relative to the isotopic composition of the modern atmosphere. Isua (Fig. 1d) and Gaoua (Fig. 1e) samples show $^{131\text{-}136}Xe$ excesses, which might be attributed to the spontaneous fission of ^{238}U although fission spectra are not decisive (Fig. S3 & S4, respectively, in Supplementary Information). Enrichment of light isotopes and depletion of heavy isotopes are consistent with mass-dependent isotopic fractionation of the underlying original component of the Earth's atmosphere assumed to be U-Xe. The Xe mass fractionation is recorded in quartz samples of different ages, and is consistent with the findings of previous studies of ancient atmosphere trapped in fluid inclusions in quartz and barite samples (Pujol et al., 2009; Pujol et al., 2011; Avice et al., 2017) and in carbon-rich material (Bekaert et al., 2018). Deviations from this mass-dependent fractionation (Fig. 1) are mainly due to fissiogenic excesses from the spontaneous fission of ^{238}U (in the case of $^{132\text{-}136}Xe$) or to ill-constrained spallation phenomena (see below). Results presented here cannot be interpreted in terms of mixing between an atmospheric and a mantle-derived component (Pepin, 2013), due to the absence of a significant ^{129}Xe excess relative to the modern atmosphere (6.8% of radiogenic $^{129}Xe^*$ excess from the decay of extinct ^{129}I in the modern atmosphere) expected in mantle components (Caffee et al., 1999). In fact, after correction for isotopic fractionation relative to U-Xe, there is a $^{129}Xe^*$ depletion of 6.6 ± 1.8 ‰ (1σ) in Barberton quartz compared to the radiogenic $^{129}Xe^*$ excess in the modern atmosphere. This observation demonstrates that Barberton samples are records of an ancient atmosphere containing lower amounts of radiogenic gases 3.3 Ga ago, which were subsequently degassed from the mantle and accumulated in the atmosphere (Avice et al., 2017). N_2-Ne-Kr isotope systematics of Barberton samples also argues against any significant mantle influence on the composition of the trapped fluids (see next section). The data presented here thus appears to record the isotopic composition of xenon in paleoatmospheres.

A depletion of ^{124}Xe, relative to any plausible mass-dependent fractionation determined using other light non-radiogenic/fissiogenic isotopes (Table 1), is observed in the case of Barberton (3.3 Ga) and Fortescue Group (2.7 Ga) samples. This depletion is unlikely to be due to an isotopic fractionation artefact during extraction, purification and analysis of the gas as crushing experiments of more recent quartz crystals (Tables S1) did not reproduce such depletion and yielded present-day atmospheric $^{124}Xe/^{130}Xe$ ratios (e.g., results for samples from Avranches (500 Ma) in Fig. S8 in Supplementary Material). These mono-isotopic depletions for Barberton and Fortescue Group samples are difficult to explain since there is no known source or nuclear process capable of producing ^{124}Xe in the Earth's interior (see Discussion in Avice et al., 2017). It is noted that, in the case of Fortescue Group Xe for example, propagation of mass fractionation computed with ^{124}Xe toward heavy isotopes ($^{131\text{-}136}Xe$) leads to $^{131\text{-}136}Xe$ excesses that are not compatible with spontaneous fission of ^{238}U or with fission of ^{244}Pu (see the mismatch for ^{132}Xe in the fission spectrum in Fig. S5 in Supplementary Material). This observation argues in favor of an abnormally low ^{124}Xe of unknown origin, rather than overestimated ^{126}Xe and ^{128}Xe excesses.

Values for the isotopic fractionation of Xe discussed in the following text were computed using the Xe isotopes listed in Table 1 and are expressed in delta notation relative to the isotopic composition of modern atmospheric Xe. Isotopic fractionations were computed using non-radiogenic isotopes only and then expanded to ^{129}Xe in the case of modern samples and to ^{131}Xe, an isotope for which potential contribution from the fission products is minimal. The isotopic fractionation of Xe (δXe_{air}) of 12.9 ± 1.2‰ u^{-1} (1σ) measured in 3.3 Ga Barberton samples is more precise and in agreement with previous data obtained for 3.0–3.1 Ga-old quartz from the Dresser Formation (Australia) (Pujol et al., 2011; Pujol et al., 2013a,b). Interestingly, it confirms that the isotopic fractionation of the atmosphere 3.3 Ga ago was lower than the value of 21 ± 3‰ u^{-1} measured in 3.5 Ga-old barite samples (Pujol et al., 2009) suggesting that the isotopic composition of atmospheric Xe has evolved over time. The quartz samples from the 2.7 Ga-old Fortescue Group yielded Xe results compatible with an isotopic fractionation of 13 ± 1‰ u^{-1} (1σ) identical within errors to the fractionation measured in Barberton samples, including a contribution of $^{131\text{-}136}Xe$ from the spontaneous fission of ^{238}U (see Fig. S5 in Supplementary

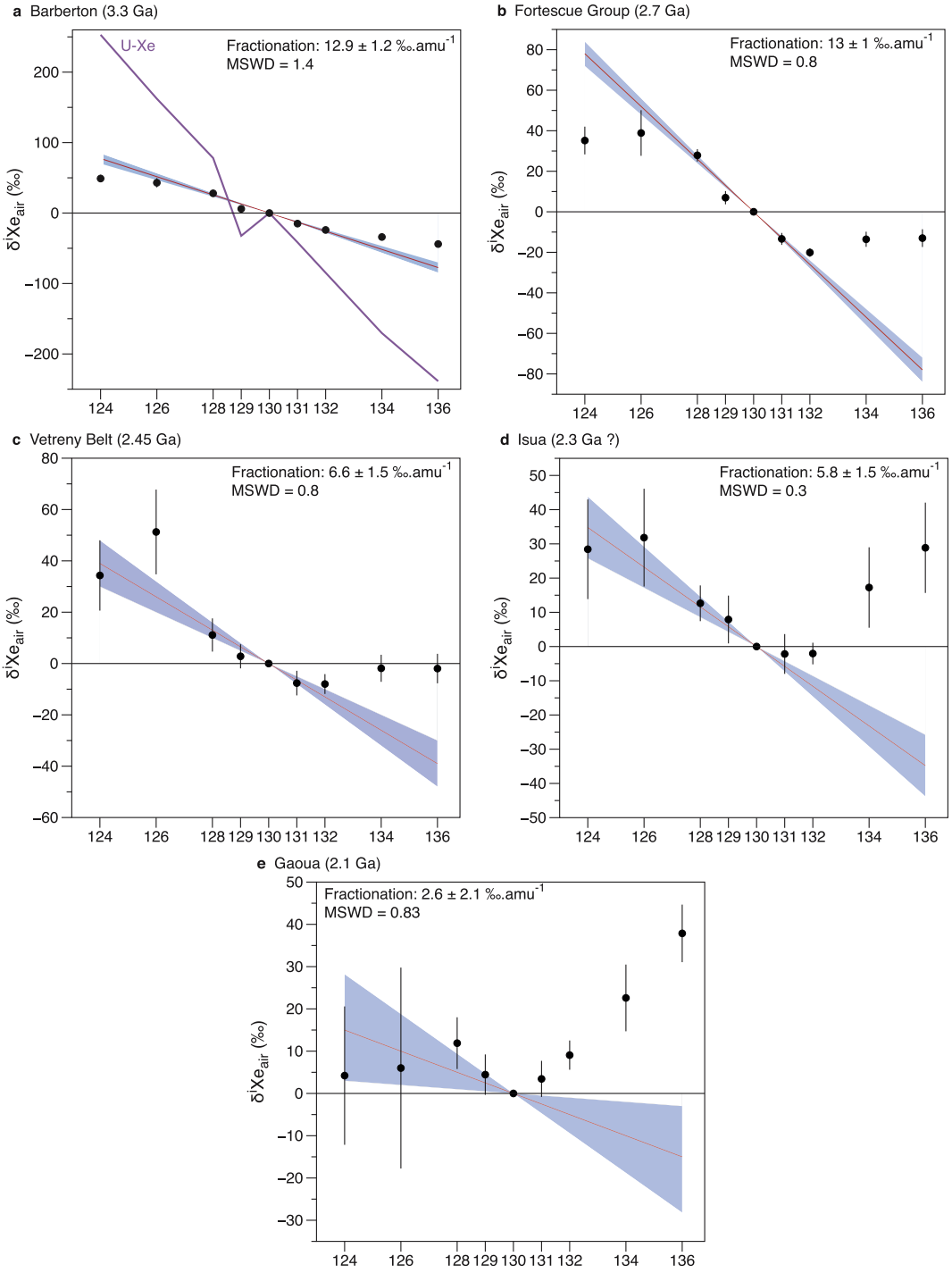

Fig. 1. Isotopic spectra of Xe released from fluid inclusions in samples from (a) Barberton, (b) Fortescue Group, (c) Vetreny Belt, (d) Isua and (e) Gaoua (see Table S1 in Supplementary Material). Note the differences in scale in b-c compared to d-e. Isotopic compositions are given using the delta notation normalized to ^{130}Xe and to the isotopic composition of the modern atmosphere ($\delta^{i}Xe_{air} = 0$ ‰): $\delta^{i}Xe_{air} = 1000 \times \left(\frac{(^{i}Xe/^{130}Xe)_{sample}}{(^{i}Xe/^{130}Xe)_{air}} - 1\right)$. For each sub-panel, red lines were computed using only the Xe isotopes listed in Table 1. The purple line in Fig. 1a corresponds to U-Xe (Pepin, 1991). Blue areas correspond to 1σ error ranges. Errors are 1σ. (For interpretation of the references to colour in this figure legend, the reader is referred to the web version of this article.)

Material). Furthermore, Xe results for Fortescue Group samples confirm that the only possible starting isotopic composition for the Earth's atmosphere is similar to the U-Xe (see the three-isotope plot in Fig. S6 in Supplementary Material). Mass-dependent fractionation of this component and addition of products from the spontaneous fission of ^{238}U are the only means to reproduce the measured ^{136}Xe/^{130}Xe ratio.

Xenon in the quartz sample from Vetreny belt (Fig. 1(c)) is fractionated by 6.6 ± 1.5‰ u^{-1} (Table 1). ^{134}Xe and ^{136}Xe excesses are consistent with production from spontaneous fission of ^{238}U (Fig. S3).

Samples from Isua show an isotopic fractionation of 5.8 ± 1.5‰ u^{-1} (Table 1, Fig. 1c) and some excesses of spontaneous fission isotopes from ^{238}U (Fig. S3). This isotopic fractionation is lower than the fractionation recorded in Barberton (3.3 Ga) and Fortescue Group (2.7 Ga) samples (≈13‰ u^{-1}).

Samples from the Quetico Belt (2.7–2.65 Ga) display small ^{128}Xe excesses relative to the modern atmosphere but uncertain $^{124,126}Xe/^{130}Xe$ ratios prevent a precise determination of the possible isotopic fractionation (Fig. S1 in Supplementary Material). The small ^{128}Xe excess is not due to double-beta decay of ^{128}Te ($\lambda = 9 \times 10^{-26}$ a^{-1}) since concomitant double-beta decay of ^{130}Te ($\lambda = 2.6 \times 10^{-22}$ a^{-1}) would have produced a significant ^{130}Xe excess that is not observed here (Pujol et al., 2009). Neutron capture on ^{127}I followed by beta decay of ^{128}I ($^{127}I(n, \gamma)^{128}I(\beta^-)$) would produce mono-isotopic ^{128}Xe excesses (Srinivasan et al., 1971). However, the abundance of iodine in Quetico Belt samples is unknown so the contribution of ^{128}Xe from this source cannot be established. A minor isotopic fractionation of 3.8 ± 2.5‰ u^{-1} is still possible even if it only relies on this ^{128}Xe excess of doubtful origin. Similarly, the isotopic fractionation of 2.5 ± 1.6‰ u^{-1} recorded in Gaoua ≈2.1 Ga-old quartz samples (Table 1, Fig. 1(d)) is mainly carried by the $^{128}Xe/^{130}Xe$ ratio that is higher than the modern one. Even though $^{124}Xe/^{130}Xe$ and $^{126}Xe/^{130}Xe$ ratios are imprecise, they are also compatible with an isotopic fractionation of this magnitude.

Carnaíba samples (2.0–1.9 Ga) do not present any resolvable isotopic fractionation (1.8 ± 2.2‰ u^{-1}) and show a ^{126}Xe excess of unknown origin (Fig. S2 in Supplementary Material). Cosmogenic production of ^{126}Xe is possible, however this process would have produced comparable ^{124}Xe excesses (Pujol et al., 2009) that are not observed. Samples from Caramal (1.7 Ga) (Fig. S7 in Supplementary Material) contain a ^{128}Xe excess possibly attributed to neutron capture on ^{127}I (similarly to Quetico Belt samples). All other isotopes are compatible with a modern air-like isotopic composition. The maximum isotopic fractionation is 0.32 ± 0.78‰ u^{-1} (Table 1). Xenon in the sample from Avranches (530 Ma) (Fig. S8 in Supplementary Material) does not show any resolvable deviation relative to the isotopic composition of the modern atmosphere. The sample from Rhynie (404 Ma) (Fig. S9 in Supplementary Material) has a Xe isotopic composition slightly enriched in light $^{124\text{-}126}Xe$ isotopes but this composition does not, within measurement precision, deviate from modern atmosphere. The maximum Xe isotope fractionations and their associated errors for Caramal, Avranches and Rhynie samples are listed in Table 1.

3.2. Neon, argon and krypton isotopes

The isotopic compositions of Kr in Barberton and Vetreny belt samples are reported in Table S2 (Supplementary Material) and are displayed in Fig. 2 where the isotopic ratios are normalized to ^{84}Kr and expressed with the delta notation relative to the isotopic composition of the modern atmosphere. The isotopic composition of Kr in Barberton and Vetreny belt quartz samples is identical to that of the modern atmosphere. If the mass fractionation recorded by Xe was extended to Kr assuming a fractionation law proportional to the square root of the masses, the isotopic fractionation of Kr should be 16.2‰ u^{-1} and 8.3‰ u^{-1} for Barberton and Vetreny belt quartz samples, respectively (Fig. 2). Therefore, the isotopic fractionation process recorded by Xe is specific to this noble gas and does not affect other noble gases. It also confirms the absence of mantle-derived fluids since mantle-derived CO_2 well-gases carry a Kr signature that is intermediate between air and a Chondritic component (AVCC-Kr) (Holland et al., 2009).

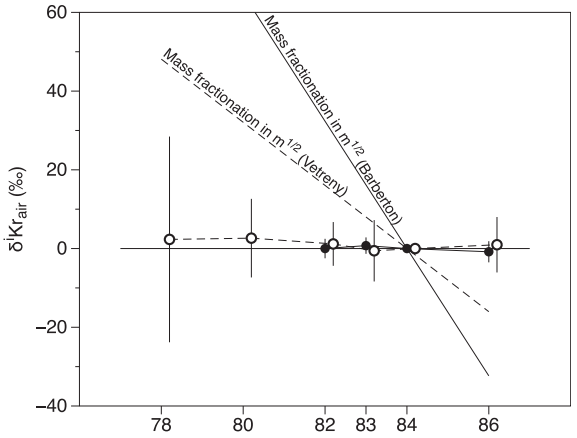

Fig. 2. Isotopic composition of Kr released from fluid inclusions in Barberton (black circles) and Vetreny belt (open circles) quartz samples (Table S2). Isotopic ratios are normalized to ^{84}Kr and to the isotopic composition of the modern atmosphere and expressed using the delta notation (in per mil): $\delta^i Kr_{air} = 1000 \times \left(\frac{(^iKr/^{84}Kr)_{sample}}{(^iKr/^{84}Kr)_{air}} - 1\right)$. The isotopic compositions do not show any deviation from the isotopic composition of the atmosphere. Propagation for Kr of the isotopic fractionation measured for Xe in Barberton (plain line) and Vetreny belt (dashed line) quartz samples and following a mass fractionation law in $m^{1/2}$ is also shown. Error at 2σ.

Results for abundances and isotopic compositions of nitrogen, argon and neon in fluid inclusions of sample BMGA3-9 (Barberton) are listed in Table 2 and given in the following text with 1σ error ranges. $^{40}Ar/^{36}Ar$ ratios are elevated with a maximum value of 978 ± 82 (crushing step #5 for sample BMGA3-9B) and a reproducible mean value of around 700, with also highly reproducible ^{36}Ar contents of 1.16×10^{-13} mol g^{-1}. This elevated $^{40}Ar/^{36}Ar$ ratio relative to the modern atmospheric ratio of 298.56 (Lee et al., 2006) cannot be explained by addition of ^{40}Ar produced in-situ by the radioactive decay of ^{40}K during 3.3 Ga, because the ^{40}K contents are too low (see Discussion in Avice et al. 2017). This demonstrates that fluids trapped in these quartz samples do not correspond directly to seawater equilibrated with the atmosphere. Assuming the initial fluid was derived from seawater, its noble gas isotopic and elemental composition was modified during interaction with crustal rocks becoming enriched in radiogenic

Table 2
Results for the N_2-Ar-Ne crushing experiments on two subsamples of Barberton (BMGA3-9 A & B). Bold values correspond to total gas released from fluid inclusions. Errors at 1σ.

Sample	Crush	$^{28}N_2$ mol g^{-1}	+/−	$\delta^{15}N$ ‰	+/−	^{36}Ar mol g^{-1}	+/−	$^{40}Ar/^{36}Ar$	+/−	$^{38}Ar/^{36}Ar$	+/−	^{22}Ne mol g^{-1}	+/−	$^{20}Ne/^{22}Ne$	+/−	$^{21}Ne/^{22}Ne$	+/−
BMGA3-9-A	#2*	1.139E-09	3.2E-11	8	3	2.35E−14	7E−16	722	56	0.187	0.019	1.24E−15	2E−17	10.05	0.11	0.031	0.003
	#3	8.30E−10	2.3E−11	3	3	1.82E−14	7E−16	604	62	0.197	0.025	8.7E−16	2E−17	9.75	0.22	0.040	0.007
	#4	9.95E−10	2.8E−11	4	4	2.78E−14	7E−16	609	41	0.188	0.016	1.09E−15	2E−17	9.45	0.16	0.028	0.003
	#5	1.007E−09	2.8E−11	−1	3	2.14E−14	7E−16	641	55	0.185	0.021	8.5E−16	2E−17	9.73	0.23	0.024	0.003
	#6	1.019E−09	2.8E−11	−6	3	1.34E−14	7E−16	840	111	0.187	0.033	4.2E−16	1E−17	9.66	0.30	0.033	0.006
	#7	8.06E−10	2.2E−11	1	3	1.15E−14	8E−16	872	134	0.188	0.039	3.6E−16	1E−17	10.35	0.35	0.041	0.004
Total		**5.797E−09**	**6.6E−11**	**1**	**2**	**1.16E−13**	**2E−15**	**690**	**28**	**0.188**	**0.009**	**4.82E−15**	**4E−17**	**9.79**	**0.08**	**0.032**	**0.002**
BMGA3-9-B	#1	1.444E−09	4.0E−11	−3	3	3.06E−14	4E−16	643	15	0.186	0.006	1.40E−15	2E−17	9.64	0.07	0.031	0.001
	#2	6.27E−10	1.7E−11	−3	4	2.02E−14	3E−16	525	20	0.191	0.009	4.6E−16	1E−17	10.09	0.22	0.023	0.016
	#3	1.318E−09	3.7E−11	−4	3	1.97E−14	3E−16	809	29	0.190	0.009	9.4E−16	1E−17	9.59	0.10	0.030	0.002
	#4	9.80E−10	2.7E−11	2	3	1.68E−14	3E−16	769	32	0.191	0.011	5.8E−16	9E−18	9.54	0.14	0.033	0.002
	#5	7.76E−10	2.2E−11	−3	3	8.24E−15	3E−16	978	82	0.193	0.022	3.6E−16	6E−18	9.37	0.18	0.034	0.002
	#6	5.73E−10	1.6E−11	3	3	1.12E−14	3E−16	663	43	0.190	0.016	1.0E−16	2E−18	9.54	0.17	0.035	0.006
	#7	3.84E−10	1.1E−11	−1	3	9.05E−15	3E−16	660	53	0.190	0.020	4.1E−17	1E−18	9.58	0.30	0.039	0.005
Total		**6.103E−09**	**6.9E−11**	**1**	**2**	**1.158E−13**	**9E−16**	**696**	**12**	**0.190**	**0.004**	**3.89E−15**	**3E−17**	**9.64**	**0.05**	**0.030**	**0.002**
Air[a]				0				298.56		0.188				9.8		0.029	

* Analysis of the first cruch had to be aborted because of high water content.
[a] Values are from Ozima and Podosek (2002) for noble gases and air is the reference for $\delta^{15}N$ so $\delta^{15}N_{air} = 0‰$.

^{40}Ar, fissiogenic $^{131\text{-}136}$Xe, etc. It is likely that the isotopic composition of non-radiogenic/fissiogenic isotopes of xenon did not change since crustal noble gases are dominated by the atmospheric component (Drescher et al., 1998). Similarly to Kr, ^{38}Ar/^{36}Ar ratios of 0.190 ± 0.004 and 0.188 ± 0.009 for samples BMGA3-9B and BMGA3-9 A, respectively, do not show any resolvable deviation from the isotopic composition of the modern atmosphere (0.1885 ± 0.0003; Lee et al. (2006)).

Ne/Ar ratios (0.03–0.04) in Barberton samples are intermediate between seawater and air values (0.015 and 0.053, respectively; Holland and Ballentine, 2006). This difference may be explained by the mixing between air or seawater and another crustal/hydrothermal component of unknown elemental composition (Marty et al., in press). However, it must be emphasized that several processes such as boiling of water, salinity, separation of a gas phase in inclusions are also known to fractionate elemental compositions of noble gases (Ballentine et al., 2002). Noble gas elemental ratios alone are thus inadequate tools here to decipher the origin of gases trapped in these fluid inclusions.

Neon isotopic ratios are displayed in a three-isotope plot in Fig. 3 where they are compared to the mantle component (^{20}Ne/^{22}Ne = 12.7–13.4; Marty (2012), Péron et al. (2017), Mukhopadhyay (2012)) and to the modern (Kennedy et al., 1990) and Archean crustal mixing lines (Lippmann-Pipke et al., 2011; Holland et al., 2013). Crushing steps and bulk values are close to the atmospheric composition. Some steps give ^{20}Ne/^{22}Ne and ^{21}Ne/^{22}Ne ratios that are lower than the present-day atmosphere. This is considered to result from under-correction of ^{22}Ne for $^{44}CO_2^{++}$ interference (see Supplementary Material). Crushing step #7 for BMGA3-9 A has a high ^{20}Ne/^{22}Ne = 10.35 ± 0.35, suggestive of mantle-derived Ne. However, this represents only 7.5% of the total ^{22}Ne released from fluid inclusions during the crushing experiment and bulk neon isotopic ratios for sample BMGA3-9 A (^{20}Ne/^{22}Ne = 9.79 ± 0.008, ^{21}Ne/^{22}Ne = 0.032 ± 0.002) are very close to atmospheric values.

3.3. Nitrogen

Marty et al. (2013) previously demonstrated by using N_2-Ar isotope systematics on 3.5 Ga old quartz samples from the Dresser Formation, Australia that, during this time, the partial pressure of atmospheric nitrogen (p_{N2}) was comparable to modern atmosphere, and thus unlikely to be 2–3 times higher as previously advocated to partially solve the faint young Sun paradox (Goldblatt et al., 2009). Here we used the same approach on results obtained on the 3.3 Ga old samples from Barberton, South Africa (Table 2). ^{40}Ar/^{36}Ar isotopic ratios versus N_2/^{36}Ar elemental ratios are displayed in the argon-mixing diagram in Fig. 4(a). Crushing steps define a linear correlation compatible with a mixing between two end-members. The first end-member has elevated N_2/^{36}Ar and ^{40}Ar/^{36}Ar ratios consistent with a crustal/hydrothermal component (Marty et al., 2013). The second end-member is considered to be 3.3 Ga-old atmosphere having a ^{40}Ar/^{36}Ar lower than modern air ($\leq$298.56) and a N_2/^{36}Ar ratio similar or even lower than the modern atmosphere ($(N_2/^{36}Ar)_{air} = 1.02\text{–}1.31 \times 10^4$ for ocean temperatures between 2 °C and 70 °C (Marty et al. (2013) and refs. therein). In Fig. 4 (a), an upper estimate of the N_2/^{36}Ar value can be obtained from the maximum feasible ^{40}Ar/^{36}Ar ratio of the Barberton atmosphere. The ^{40}Ar/^{36}Ar value 3.3 Ga-ago is not well-constrained, however atmospheric evolution models indicate this ratio has increased over time, thus a maximum value is given by the present day atmospheric value of 298.56. The maximum N_2/^{36}Ar is therefore given by the

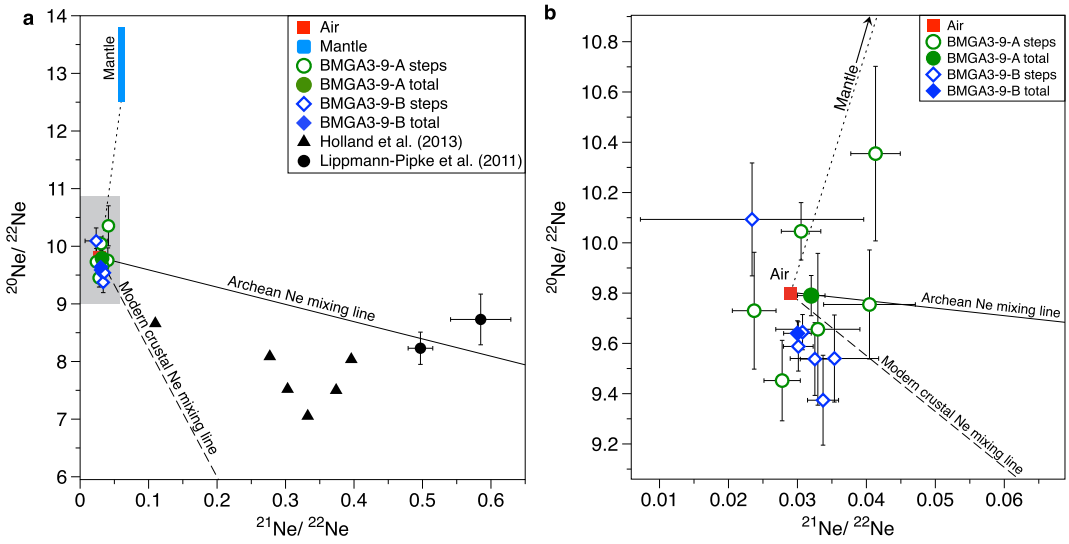

Fig. 3. Three-isotope plot of Ne for crushing experiments on BMGA3-9 subsamples (green (A) and blue (B)) (see data in Table 2). Open symbols correspond to crushing steps and filled symbols to total extractions. The blue range corresponds to possible mantle ^{20}Ne/^{22}Ne ratios (12.5–13.7) (Yokochi and Marty, 2004). Modern crustal Ne mixing line corresponds to addition of crustal nucleogenic Ne (Kennedy et al., 1990). The Archean mixing line and associated black-filled circles are from analyses by Lippmann-Pipke et al. (2011). Data obtained on Precambrian fluids by Holland et al. (2013) are indicated with black-filled triangles. Grey range in (a) corresponds to the zoom in sub-panel (b). Errors at 1σ. (For interpretation of the references to colour in this figure legend, the reader is referred to the web version of this article.)

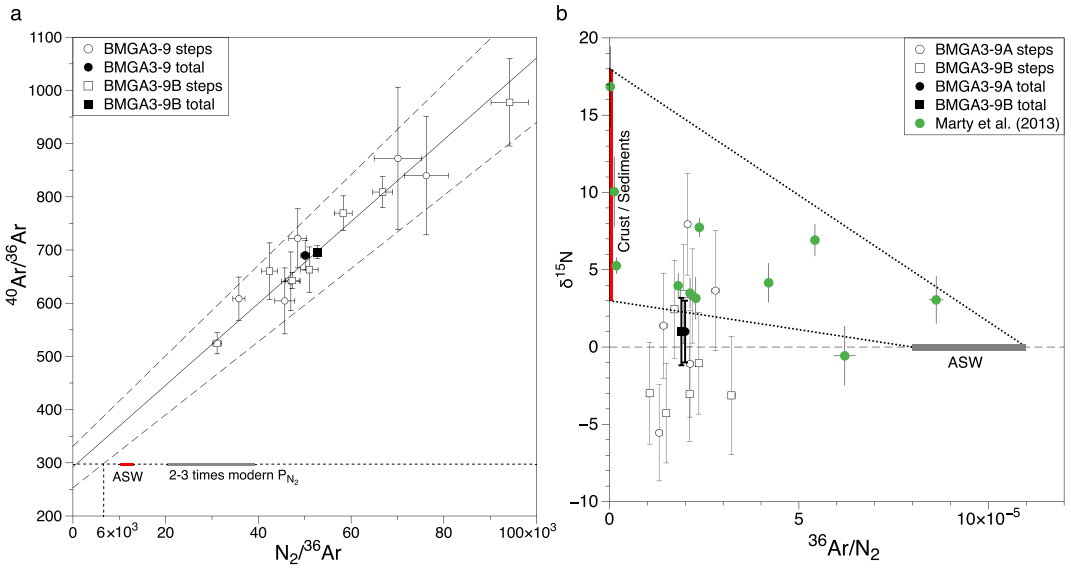

Fig. 4. Nitrogen-Argon mixing diagrams. (a) Argon-mixing diagram for crushing experiments on BMGA3-9 sub-samples (see data in Table 2). Crushing steps define a linear correlation (black line and 1σ error range defined by dashed lines) between an atmospheric end-member similar to the modern atmosphere, and a hydrothermal component. An atmospheric end-member with a maximum $N_2/^{36}Ar$ ratio of 6.6×10^3 is envisaged (see text). (b) Nitrogen isotopes mixing diagram. Empty symbols correspond to individual crushing steps and filled symbols correspond to total gas (sum of all crushing steps). Data are compatible with a mixing between a modern-like component (air or ASW) and a crustal/sedimentary-derived component. Green-filled circles correspond to data from Marty et al. (2013). Range for $\delta^{15}N$ in crust or sediments are from Cartigny and Marty (2013) and refs. therein. Errors at 1σ. (For interpretation of the references to colour in this figure legend, the reader is referred to the web version of this article.)

intersection of the lower limit 1σ uncertainty on the linear correlation shown in Fig. 4(a) with this $^{40}Ar/^{36}Ar$ ratio, yielding a value of 6.6×10^3. This $N_2/^{36}Ar$ indicates that the partial pressure of nitrogen in the 3.3 Ga-old atmosphere was likely lower than the modern one (at a 1σ level of precision) and not compatible with a partial pressure 2–3 times the modern one at the 2σ level of precision.

Nitrogen isotopic compositions are displayed in a nitrogen-mixing diagram ($\delta^{15}N$ vs. $^{36}Ar/N_2$) in Fig. 4b. Nitrogen isotopic compositions are expressed using the delta notation ($\delta^{15}N$) relative to the isotopic composition of modern air ($\delta^{15}N_{air} = 0$ ‰). Values for modern crust and sediments (3‰ < $\delta^{15}N$ < 18‰) are from Cartigny and Marty (2013) and refs. therein. Crushing steps and total extractions are clustered on $^{36}Ar/N_2$ values of about 2×10^{-5} with a total $\delta^{15}N$ value of 1 ± 2 ‰ (1σ). In agreement with Marty et al. (2013) (green-filled circles in Fig. 4 (b)), our results are consistent with mixing between an ancient atmospheric component with $\delta^{15}N \approx 0$‰ and a crustal/sedimentary end-member. Our results confirm that the nitrogen isotope composition of the Earth's atmosphere has remained stable over at least the last 3.3 Ga. This has implications for the presence of a substantial magnetic field over this duration that was sufficiently strong to inhibit isotopic fractionation of atmospheric nitrogen through electron impacts, charge exchanges and photoionization during atmospheric erosion (Lichtenegger et al., 2010).

4. DISCUSSION

The N_2-Ar-Ne measurements demonstrate that fluids trapped in the analyzed quartz samples are dominated by dissolved (paleo)atmospheric noble gases, modified to some extent by the interaction with surrounding crustal rocks. Neon and Kr isotopic results do not show the contribution of a mantle-derived component (Pujol et al., 2013a,b) as was established by the absence of ^{129}Xe excesses from the decay of extinct ^{129}I (see previous section and discussion in Avice et al. (2017)). Xenon is the only element showing large isotope differences with respect to modern atmospheric composition and the remaining discussion will be devoted to this aspect.

4.1. Evolution of the isotopic composition of atmospheric xenon

Xenon results obtained in this study are summarized in Fig. 5 and Table 1. Values of isotopic fractionation (δXe_{air} in ‰ u^{-1}) were computed for Xe released from fluid inclusions in samples of different ages. Results from previous studies (Srinivasan, 1976; Meshik et al., 2001; Pujol et al., 2009; Pujol et al., 2011; Holland et al., 2013; Pujol et al., 2013a; Avice et al., 2017; Bekaert et al., 2018) are also shown. The results enable the isotopic evolution of atmospheric Xe to be tracked with time. Interestingly, samples from Barberton (South Africa) dated at 3.30 ± 0.05 Ga display a similar fractionation (12.9 ± 1.2‰ u^{-1}) as samples from the Fortescue Group (Australia) (13.0 ± 1.2‰ u^{-1}) that are younger than 2.74 Ga. This observation suggests that the isotopic evolution of atmospheric Xe may have slowed or stopped for over 500 Myrs. Alternatively, this apparent plateau could also be caused by uncertainties in the formation ages of the samples analyzed. A recent study shows that Xe trapped in Archean kerogen from a 2.95 Ga-

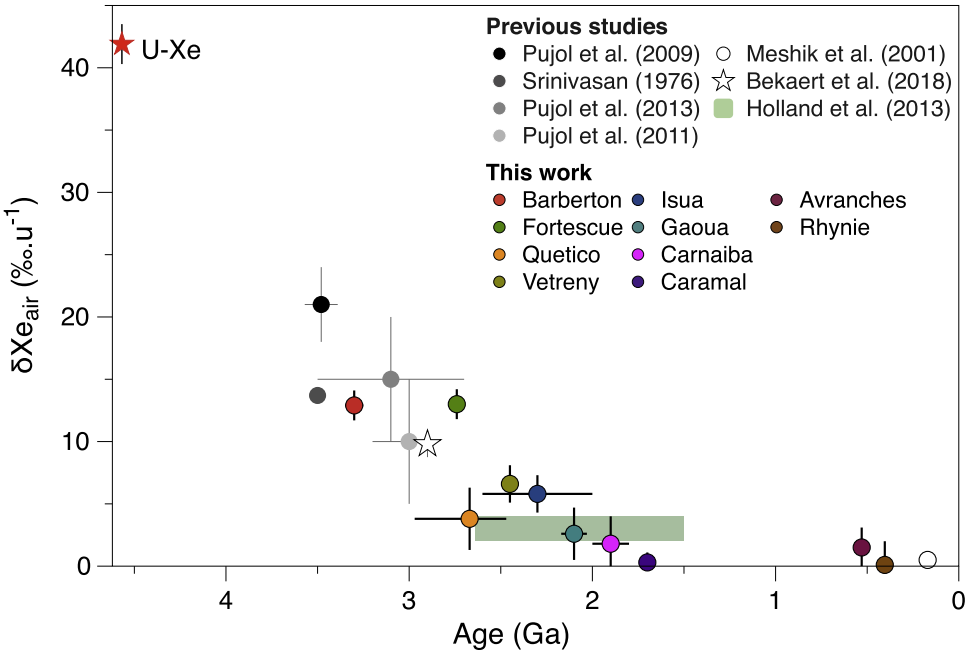

Fig. 5. Evolution of the isotopic fractionation of atmospheric Xe with time. The red-filled star represents the isotopic fractionation calculated for light isotopes of U-Xe relative to the modern atmosphere (Ott, 2014). Black, grey-tone, white circles, the white star and the green range are results from previous studies (see text and refs. therein). Color-filled circles are results from the present study (see Table 1). The point (white star) from Bekaert et al. (2018) has been shifted from 3 Ga to 2.9 Ga for ease of visibility. Errors at 1σ. (For interpretation of the references to colour in this figure legend, the reader is referred to the web version of this article.)

old lithology is fractionated by 9.8 ± 1.1‰ u^{-1} (Bekaert et al., 2018), lower than the two above values for 3.3 and 2.7 Ga. Future studies focusing on well-dated 3.3–2.7 Ga-old samples will help establish whether the evolution of the isotopic composition of atmospheric Xe remained constant during this period of time. The isotopic fractionation of 5.8 ± 1.5‰ u^{-1} recorded in the sample from Isua is intermediate between the isotopic fractionation recorded at 2.7 Ga (≈13‰ u^{-1}) and that at 2.1 Ga (≈2.1‰ u^{-1}). It is consistent with the isotopic fractionation recorded by the 2.45 Ga-old Vetreny belt sample (6.5 ± 1.5‰ u^{-1}). In a model of a progressive decrease of Xe isotopic fractionation with time (see next section), this observation tends to indicate that Isua metacarbonate samples are more likely ca. 2.3 Ga-old than ≥3.7 Ga old. The age of 2.3 Ga may correspond to the resetting event recorded by Sm-Nd dating of rocks from this area (Blichert-Toft and Frei, 2001). Isotopic fractionation of atmospheric Xe may have reached its present value between 2.1 Ga ($\delta Xe_{air} = 2.1 \pm 1.6$‰ u^{-1} for samples from Gaoua) and 1.7 Ga (0.32 ± 0.89‰ u^{-1} for samples from Caramal). Because of the scarcity of well-preserved rocks older than 3.5 Ga, there is, up to now, no constraints on the earlier stages of isotopic evolution.

This evolution could result from escape of xenon to space following a Rayleigh distillation type process (Fig. 5) (Marty, 2012; Hébrard and Marty, 2014). During this process, the progressive escape of Xe atoms from the atmosphere to space is accompanied by an instantaneous isotopic fractionation α (Pujol et al., 2011; Marty, 2012; Hébrard and Marty, 2014). Such isotope fractionation could occur during Xe ion trapping in forming organic haze (Marrocchi et al., 2011; Hébrard and Marty, 2014; Kuga et al., 2015) or directly during an escape mechanism (Zahnle and Kasting, 1986). The Rayleigh distillation equation for Xe isotope fractionation is:

$$\frac{({}^{i}Xe/{}^{130}Xe)_{t}}{({}^{i}Xe/{}^{130}Xe)_{initial,4.56\ Ga\ ago}} = f^{(130-i)\alpha} \quad (1)$$

where f is the depletion factor of the reservoir (the atmosphere), α is the instantaneous fractionation factor (u^{-1}), and $({}^{i}Xe/{}^{130}Xe)_{t}$ and $({}^{i}Xe/{}^{130}Xe)_{initial,4.56\ Ga\ ago}$ are the isotopic ratios of Xe normalized to ^{130}Xe for the atmosphere at age t and for the initial composition, that is U-Xe, 4.56 Ga ago, respectively.

Remarkably, the isotopic composition of Xe in the modern atmosphere together with its 23-fold depletion ($f = 0.043$) (Pepin, 1991) are compatible with a Rayleigh distillation evolution with an instantaneous fractionation factor α of 0.012 u^{-1} *i.e.* 12‰ u^{-1} (Fig. 6(a) and (b)). This value is fully consistent with the range of isotopic fractionation (10 ± 4‰ u^{-1}) observed in laboratory experiments when ionized Xe is trapped in organic matter (Marrocchi et al., 2011; Kuga et al., 2015). It is notable that Eq. (1) assumes a constant instantaneous fractionation factor, and this may not be the case since the physico-chemical process(es) behind selective atmospheric escape of Xe may have varied over time (see next section). The instantaneous fractionation factor of 12‰ u^{-1} must thus be considered as an integrated isotopic fractionation throughout the depletion interval. Furthermore, this simple model makes the assumption that the original Earth's atmosphere contained

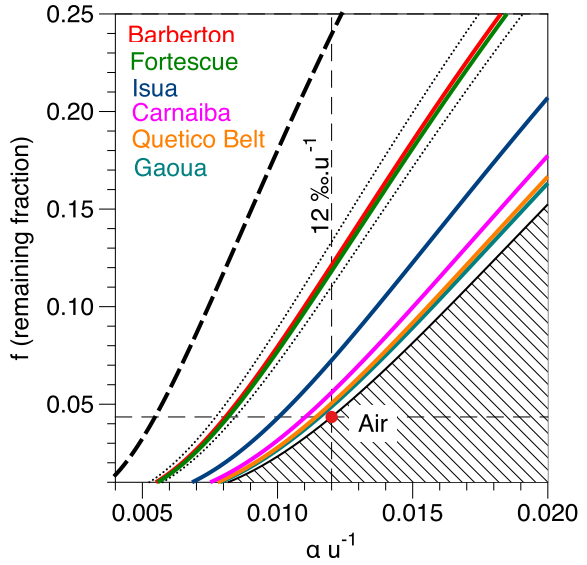

Fig. 6. Remaining fractions for isotopic fractionations of Xe measured in this study if the atmosphere evolved following a Rayleigh distillation process (see Table 1). Dotted lines correspond to the 1σ error on the fractionation measured for Barberton Xe (Table 1). The result from a previous study (Pujol et al., 2011) is shown for comparison (thick black dashed line). (For interpretation of the colours in this figure, the reader is referred to the web version of this article.)

chondrite-like abundances of noble gases. However, a cometary contribution for the Earth's atmosphere during late stages of planetary accretion is plausible (Marty et al., 2017, 2016) and heavy noble gas elemental abundances in this possible cometary contribution remain unknown. By using the generalized notation $\delta Xe_{U\text{-}Xe}$, which is the measured isotopic fractionation relative to the U-Xe, the starting composition (Pepin, 1991), the remaining fraction f can also be expressed as:

$$f = \left(1 - \frac{\delta Xe_{U-Xe}}{1000}\right)^{\frac{1}{\alpha}} \quad (2)$$

Fig. 6(a) depicts the remaining fraction (f) of Xe in the atmosphere versus the instantaneous fractionation factor (α) for each set of samples analyzed in this study. The error range at 1σ is shown for Barberton. Remaining fractions and depletion factors of the atmosphere for $\alpha = 12‰\ u^{-1}$ are listed in Table 1 with an error bar at 1σ corresponding to the propagation of the uncertainties on the isotopic fractionation relative to the starting U-Xe composition. Xenon in Barberton and Fortescue Group samples show identical isotopic fractionations corresponding to a remaining fraction (f value) of the original atmosphere of 11 ± 1%. The depletion factors computed for Xe in Quetico Belt, Isua, Vetreny belt, Carnaíba, and Gaoua samples are indistinguishable within their errors (Table 1) and vary between 12 and 25.

The existence of an isotopic fractionation of Xe in the atmosphere still present ca. 2 Ga ago has important implications for interactions between the Earth's mantle and the atmosphere. Parai and Mukhopadhyay (2015) noted that the isotopic composition of mantle-derived gases can only by explained by incorporating a non-fractionated modern-like air component in the mantle. This suggests that if fractionated ancient air had been initially subducted early in the Earth's mantle, it would had been re-degassed in the atmosphere during mantle overturn (Coltice et al., 2009). Parai and Mukhopadhyay (2015) considered only the replacement of the atmospheric component by a fractionated component similar to that measured by Pujol et al. (2011). Thus, there remains a possibility for progressive addition of subducted components having a Xe isotopic composition evolving towards the modern value.

4.2. Possibilities of escape and relation to the evolution of the atmosphere

Results presented in this study call for a long-term escape of Xe from the atmosphere to space. However, the simple Rayleigh distillation model presented in the previous section does not provide insight into the mechanism responsible for Xe escape.

Early models of xenon-hydrogen escape that attempted to solve the xenon paradox required a strong EUV flux (*e.g.* Hunten et al. (1987)) indicating that such a process was only possible early in Earth's history (Zahnle and Kasting, 1986). Furthermore, complex models of differential degassing and/or Xe retention in the silicate Earth were necessary to selectively deplete and isotopically fractionate Xe while not affecting Kr (Pepin, 1991). In a hydrodynamic escape model, the escape flux of heavier species (i = Xe) transported by escaping hydrogen is governed by Eq. (3):

$$\phi_i = \left(\phi_H - \frac{(m_i - m_H)gb(i,H)}{kT}\right) f_i \quad (3)$$

where ϕ_H, m_H and ϕ_i, m_i are the escape fluxes ($cm^{-2}\ s^{-1}$) and masses of hydrogen and of species i, respectively, g is the acceleration due to the gravitational field (980.65 $cm^2\ s^{-1}$), k is the Boltzmann constant, T is the temperature of the exobase (in Kelvin), $b(i, H)$ is the binary diffusion coefficient ($cm^{-1}\ s^{-1}$) equal to $4.5 \times 10^{17}\ T^{0.71}$ (Zahnle and Kasting, 1986) in the case of neutral ^{130}Xe escaping with H_2 and f_i is the mixing ratio of Xe divided by the mixing ratio of hydrogen. The high value of $b(i, H)$ and the high mass of ^{130}Xe lead to extreme ϕ_H values required for Xe to escape. Zahnle (2015) concluded that Xe escape in its neutral form was possible only in the first 100 Ma of Earth's history when the EUV flux from the young Sun was sufficiently strong (>300 times the modern one) to drive a significant hydrogen-driven escape of neutral Xe. However, our results demonstrate that, if this escape and fractionation hypothesis applies, then a mechanism for Xe escape which is still ongoing ca. 2.1 Ga ago, has yet to be found.

Zahnle (2015, 2018) provided a theoretical framework explaining the progressive escape of Xe from an hydrogen-rich early atmosphere. In his model, Xe escapes as an ion, because (i) Xe is relatively easily ionized due to

enhanced EUV flux from the young Sun (Claire et al., 2012) and (ii) Xe^+ radiative recombination to neutral Xe is very slow. When ionized, Xe^+ can interact with H^+ protons via the strong Coulomb force. It effectively decreases the binary diffusion coefficient $b(Xe^+, H^+)$ by several orders of magnitude compared to the case of neutral Xe. Under these conditions a hydrogen escape flux two or three orders of magnitude smaller than in the neutral gas is sufficient for Xe^+ ions to escape. As with the hydrodynamic escape of neutrals, this escape mechanism is mass fractionating since all isotopes are dragged by protons with the same force but heavy isotopes are more gravitationally bound compared to light ones. Hydrogen escape fluxes large enough to drive Xe escape can occur from an early Earth atmosphere containing as little as 1% CH_4 or H_2. Although this is a much higher escape flux than today, it is well within the range of CH_4 or H_2 mixing ratios expected for the Earth during the Archean eon (*e.g.* Catling et al., 2001). The presence of a strong magnetic field in the past (Tarduno et al., 2014) might have also favored this escape. Indeed, Zahnle (2015) advocated that Xe^+ ions would escape preferentially from Earth's magnetic poles where open magnetic lines can channel the free escape of ions. However, most of the parameters governing this coupled hydrogen/xenon escape - the hydrogen mixing ratio in the atmosphere, temperature, ionization fraction, magnetic field strength etc. - are still poorly constrained.

Catling et al. (2001) and Zahnle et al. (2013) argued that hydrogen escape is the main mechanism that drove the oxidation of the Earth's atmosphere. Even if oxygenic photosynthesis occurred prior to the great oxygenation event (*e.g.* Planavsky et al. (2014)), in their scenario H_2 escape was responsible for oxidizing the surface reservoirs until O_2 became chemically stable in the atmosphere. If so, progressive isotopic fractionation of Xe in the past may have evolved in parallel with the progressive oxidation of surficial reservoirs of the Earth.

Fig. 7 depicts the evolution of the isotopic composition of Xe determined in this study (cf. Fig. 5) compared to: (a) the record of $\Delta^{33}S$ in sedimentary rocks (compilation by Johnston, 2011); (b) a recent model of the progressive oxygenation of the Earth's atmosphere (Lyons et al., 2014) and; (c) impact and super-plume events occurring over Earth's geological history (Abbott and Isley, 2002; Reimold and Koeberl, 2014). Sulfur mass-independent isotopic fractionation (S-MIF) ceased sometime between 2.45 and 2.32 Ga, whereas the isotopic fractionation of Xe seems to have continued to evolve until 2 Ga. Disappearance of S-MIFs is usually linked to the very beginning of the oxygenation of the Earth's atmosphere (Fig. 7(b)) because only minute amounts of oxygen in the atmosphere ($>10^{-5}$ present atmospheric level; Pavlov and Kasting (2002)) prevented the preservation of a $\Delta^{33}S$ record in sedimentary rocks (Farquhar and Wing, 2003). Sulfur isotopes are thus powerful tracers of the very beginning of the oxygenation. Abundant O_2 can prevent Xe escape as an ion because the charge exchange reaction between O_2 and Xe^+ will neutralize Xe ions (Anicich, 1993). If hydrogen escape was driving xenon escape and isotopic fractionation as proposed above, termination of the isotopic fractionation of

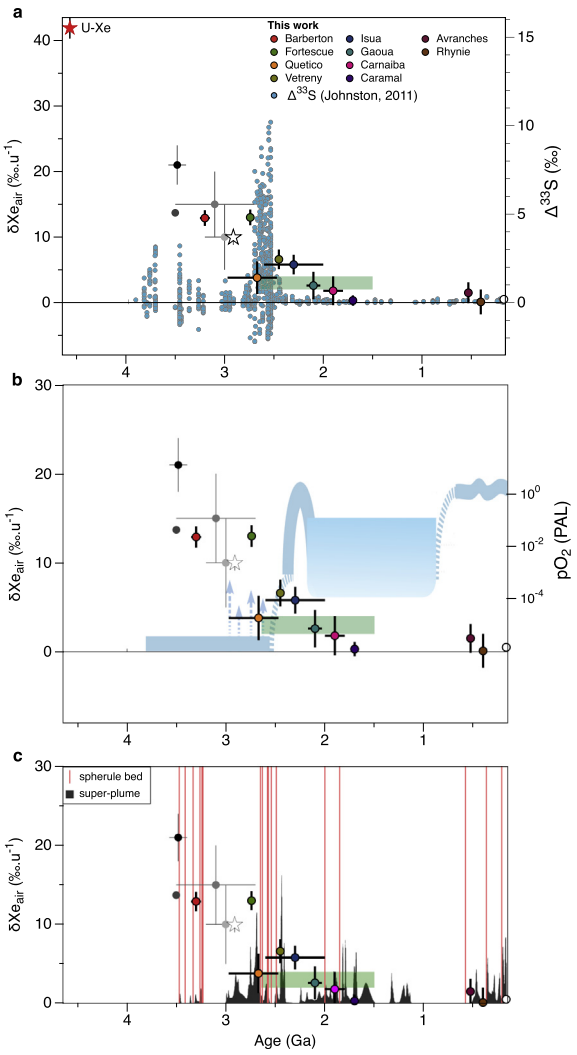

Fig. 7. Evolution of the isotopic composition of xenon (in a, b & c) compared to other isotopic signatures and significant events over Earth's geological history: (a) $\Delta^{33}S$ measured in the geological record (data are from Johnston, 2011). A mass-independent fractionation signal is present prior to 2.45 Ga. (b) Evolution of the oxygen level in the Earth's atmosphere. Figure adapted from Lyons et al. (2014). Blue arrows indicate times where there were possible whiffs of oxygen present in the atmosphere (Anbar et al., 2007). The blue range depicts the model of oxygenation presented by Lyons et al. (2014). (c) Occurrences of spherule beds (compiled by Reimold and Koeberl, 2014) indicative of major impacts (vertical red lines) and time series of super-plume events compiled by Abbott and Isley (2002). (For interpretation of the references to colour in this figure legend, the reader is referred to the web version of this article.)

Xe between 2.2 and 2.0 Ga Ga may signal a pronounced decrease in hydrogen escape and the onset of moderate oxygen levels (between 10^{-4} and 10^{-2} the present atmospheric level, Fig. 7(b)). We highlight that these moderate oxygen levels would also have prevented the development of organic hazes that may be necessary to fractionate Xe isotopes (Hébrard and Marty, 2014). In this context, the potential quiescent time between 3.3 Ga and 2.7 Ga for

Xe isotopic fractionation (Fig. 5), which is also recorded by sulfur isotopes (Fig. 7(a)), might be linked to "whiffs" of oxygen (Fig. 7(b); Anbar et al., 2007)) causing brief stops in the production of organic hazes and/or preventing the penetration of UV photons in the atmosphere responsible for ionization and escape of Xe and photolysis of sulfur. To extend the comparison, the sharp drops in the isotopic fractionation of atmospheric Xe between 3.5 and 3.3 Ga and between 2.7 and 2.5 Ga are concomitant with the presence of massive S-MIF signatures in the sedimentary record (and thus photolysis activity in the atmosphere) possibly linked to enhanced flux of SO_2 to the atmosphere during the subaerial emplacement of large igneous provinces (Philippot et al., 2012; Havig et al., 2017).

4.3. Mars-Xe and alternative models for atmospheric evolution

Although the progenitor of Martian atmospheric Xe is probably Solar Xe (e.g. Conrad et al., 2016; Avice et al., 2018) whereas for the Earth atmospheric Xe it is U-Xe (Pepin, 1991), the isotopic fractionation patterns relative to their respective progenitors for both planets are similar ($\approx$30–40‰ u^{-1}) even if the isotopic composition of Martian atmospheric xenon evolved at a faster rate (Cassata, 2017). An hydrogen-Xe^+ escape mechanism might have also been operative on Mars since some H_2 may have been present in its early atmosphere and later escaped through hydrodynamic escape mechanisms (Ramirez, 2013).

However, it is unexpected to measure a comparable value for the isotopic fractionation of modern atmospheric Xe on both planets since parameters governing the escape (hydrogen escape flux, EUV flux to ionize Xe, magnetic field strength, initial abundances of Xe) were probably very different due to the differences in distance to the Sun and to the distinct geological histories of both planets. One may thus expect to measure different isotopic fractionations of Xe in the planetary atmospheres. The similarity for Xe in the atmosphere of Mars and Earth raises an alternative model for the evolution of atmospheric Xe isotopes related to a progressive contribution of volatile-rich bodies to the terrestrial atmospheres. In this model, both atmospheres started with chondritic or solar Xe signatures. Volatile-rich bodies might have carried a U-Xe component (Marty et al., 2017) (or a solar component for Mars; Conrad et al. (2016), Avice et al. (2018)) that was already isotopically fractionated to a similar extent than modern atmospheric xenon, but involving a process that took place in a different environment, e.g. in the solar nebula (Kuga et al., 2015) or inside porous bodies (Ozima and Nakazawa, 1980; Zahnle et al., 1993). Progressive contribution of these bodies to the atmosphere would have shifted the isotopic fractionation from chondritic/solar to modern values. In this case, the starting isotopic composition for the Martian atmosphere might have been closer to solar Xe than to U-Xe, as a solar-like component has been measured in the Martian meteorite Chassigny (Ott, 1988). If this progressive contribution of fractionated Xe did occur, then additions from major impact events, as inferred from the presence of spherule beds (Reimold and Koeberl, 2014), potentially released fractionated U-Xe in the Earth's atmosphere, and mantle degassing episodes contributing chondritic-derived Xe, are two important processes to understand (Fig. 7(c)). Interestingly, important shifts in the isotopic composition of atmospheric Xe seem to be temporally correlated with major impact events present in the 3.5–3.3 Ga and 2.7 to ca. 2 Ga intervals, for example (Fig. 7(c)). However, the impact record is under-constrained due to preservation issues and sampling bias. Furthermore, such a model does not explain why Earth and Mars atmospheres show similar depletions in Xe relative to Chondritic abundances. Concerning a possible link between mantle activity and xenon isotope fractionation, we note that there is no straightforward correlation between the evolution of the isotopic composition of atmospheric xenon and the occurrence of super-plume events (Fig. 7(c), Abbott and Isley, 2002).

In this context, measuring the isotopic composition and the abundance of Xe (and Kr) in the atmosphere of Venus would be of great interest. A direct comparison with Earth and Mars would help to further constrain what are the physical processes causing progressive isotopic fractionation since the three planets present very different characteristics (mass, distance from the Sun, degassing history, atmospheric composition, magnetic field).

5. CONCLUSIONS

Results presented in this study confirm that the isotopic composition of xenon in the Earth's atmosphere is recorded in fluid inclusions of ancient quartz samples.

The isotopic composition of xenon underwent a long-term evolution from a primordial composition similar to U-Xe, as shown by Barberton and Fortescue Group samples, towards the isotopic fractionation characteristic of the modern atmosphere. The present-day isotopic composition was reached between 2.1 and 1.7 Ga. Such a long-term evolution needs to be incorporated in models to account for the xenon paradox (elemental depletion and isotopic fractionation) and originally based on an early atmospheric escape of Xe. An escape mechanism based on hydrogen escape coupled with the ionization of Xe is proposed. Termination of the isotopic fractionation of Xe may coincide with the end of the hydrogen escape which has previously been suggested to explain the progressive oxygenation of the Earth's atmosphere (Zahnle et al., 2013). Atmospheric Xe might thus be an indirect proxy of the oxidation of the Earth atmosphere.

A modeling effort of coupled Xe^+-H^+ escape may provide important insights into the mechanism for long-term escape and isotopic fractionation of Xe. In addition, measuring the isotopic composition of Xe in Venus atmosphere is essential as it would provide, in addition to Martian Xe, a third element of comparison to understand what are the processes and acting factors required to progressively fractionate atmospheric Xe.

DECLARATION OF INTEREST

None.

ACKNOWLEDGMENT

This study was funded in Nancy (France) by the European Research Council under the European Community's Seventh Framework Programme [FP7/2007-2013 grant agreement No. 267255 to B.M.]. Samples from Barberton were recovered thanks to the International Continental Scientific Drilling Program (ICDP). Francis & Isabelle Avice, Elodie Le Mignot, Antonin Richard, Gaston Giuliani and Marie-Christine Boiron are acknowledged for providing samples analyzed in this study. Collection of samples from the Vetreny belt is a Stable Isotope laboratory at University of Oregon effort. Yves Marrocchi is thanked for scientific interactions. Ken Farley is acknowledged for support during preparation of this manuscript. Laurent Zimmermann is gratefully acknowledged for technical mentorship and assistance. Rainer Wieler and an anonymous reviewer are thanked for their constructive comments and suggestions. We thank Nicolas Dauphas for his editorial handling. This is CRPG contribution #2583.

APPENDIX A. SUPPLEMENTARY MATERIAL

Supplementary data associated with this article can be found, in the online version, at https://doi.org/10.1016/j.gca.2018.04.018.

REFERENCES

Abbott D. H. and Isley A. E. (2002) The intensity, occurrence, and duration of superplume events and eras over geological time. *J. Geodyn.* **34**, 265–307. https://doi.org/10.1016/S0264-3707(02)00024-8.

Anbar A. D., Duan Y., Lyons T. W., Arnold G. L., Kendall B., Creaser R. A., Kaufman A. J., Gordon G. W., Scott C. T., Garvin J. and Buick R. (2007) A whiff of oxygen before the great oxidation event?. *Science* **317** 1903–1906. https://doi.org/10.1126/science.1140325.

Anicich V. G. (1993) A survey of bimolecular ion-molecule reactions for use in modeling the chemistry of planetary atmospheres, cometary comae, and interstellar clouds. *Astrophys. J. Suppl. Ser.* **84**, 215–315. https://doi.org/10.1086/191752.

Arndt N. T., Wilson A., Hofmann A., Mason P., Bau M., Byerly G. and Chunnett G. (2012) Peering into the cradle of life: scientific drilling in the Barberton Greenstone Belt. *Sci. Drill.* **13**, 71.

Avice G., Marty B. and Burgess R. (2017) The origin and degassing history of the Earth's atmosphere revealed by Archean xenon. *Nat. Commun.* **8**, 1–9. https://doi.org/10.1038/ncomms15455.

Avice G., Beakert D. V., Chennaoui-Aoudjehane H. and Marty B. (2018) Noble gases and nitrogen in Tissint reveal the composition of the Mars atmosphere. *Geochem. Persp. Lett.* **6**, 11–16. https://doi.org/10.7185/geochemlet.1802.

Ballentine C. J., Burgess R. and Marty B. (2002) Tracing fluid origin, transport and interaction in the crust. *RiMG* **47**, 539–614. https://doi.org/10.2138/rmg.2002.47.13.

Baratoux L., Metelka V., Naba S., Ouiya P., Siebenaller L., Jessell M. W., Naré A., Salvi S., Béziat D. and Franceschi G. (2015) Tectonic evolution of the Gaoua region, Burkina Faso: implications for mineralization. *J. Afr. Earth Sci.* **112**, 419–439. https://doi.org/10.1016/j.jafrearsci.2015.10.004.

Basford J. R., Dragon J. C., Pepin R. O., Coscio M. R., and Murthy V. R. (1973) Krypton and Xenon in lunar fines. Proceedings of the 4th Lunar Science Conference, 1915–1955.

Bekaert D. V., Avice G., Marty B., Henderson and Gudipati M. S. B. (2017) Stepwise heating of Lunar anorthosites 60025, 60215, 65315 possibly reveals an indigenous noble gas component on the Moon. *Geochim. Cosmochim. Acta* **218**, 114–131. https://doi.org/10.1016/j.gca.2017.08.041.

Bekaert D. V., Broadley M. W., Delarue F., Avice G., Robert F. and Marty B. (2018) Archean kerogen as a new tracer of atmospheric evolution: Implications for dating the widespread nature of early life. *Sci. Adv.* **4**, 1–8. https://doi.org/10.1126/sciadv.aar2091.

Blichert-Toft J. and Frei R. (2001) Complex Sm-Nd and Lu-Hf isotope systematics in metamorphic garnets from the Isua supracrustal belt, West Greenland. *Geochim. Cosmochim. Acta* **65**, 3177–3189. https://doi.org/10.1016/S0016-7037(01)00680-9.

Caffee M. W., Hudson G. B., Velsko C., Huss G. R., Alexander E. C. Jr and Chivas A. R. (1999) Primordial Noble Gases from Earth's Mantle: Identification of a Primitive Volatile Component. Science 285, 2115–2118. https://doi.org/ 10.1126/science.285.5436.2115.

Card K. D. (1990) A review of the Superior Province of the Canadian Shield, a product of Archean accretion. *Precambr. Res.* **48**, 99–156. https://doi.org/10.1016/0301-9268(90)90059-Y.

Cartigny P. and Marty B. (2013) Nitrogen isotopes and mantle geodynamics: the emergence of life and the atmosphere-crust-mantle connection. *Elements* **9**, 359–366. https://doi.org/10.2113/gselements.9.5.359.

Cassata W. S. (2017) Meteorite constraints on Martian atmospheric loss and plaeoclimate. *Earth Planet. Sci. Lett.* **479**, 322–329. https://doi.org/10.1016/j.epsl.2017.09.034.

Catling D. C. (2014) The Great Oxidation Event transition. In Treatise on Geochemistry (Second Edition). Elsevier, Oxford. pp. 177–195. https://doi.org/10.1016/B978-0-08-095975-7.01307-3.

Catling D. C., Zahnle K. J. and McKay C. P. (2001) Biogenic methane, hydrogen escape, and the irreversible oxidation of early earth. *Science* **293**, 839–843. https://doi.org/10.1126/science.1061976.

Chantraine J., Auvray B., Brun J. P., Chauvel J. J. and Rabu D. (1994) Introduction. In Pre-Mesozoic Geology in France and related areas (eds. J. Chantraine, J. Rolet, D. S. Santallier, and A. Piqué). pp. 75–80.

Cheilletz A., Féraud G., Giuliani G. and Ruffet G. (1993) Emerald dating through 40Ar/39Ar step-heating and laser spot analysis of syngenetic phlogopite. *Earth Planet. Sci. Lett* **120**, 473–485. https://doi.org/10.1016/0012-821X(93)90258-B.

Claire M. W., Sheets J., Cohen M., Ribas I., Meadows V. S. and Catling D. C. (2012) The evolution of solar flux from 0.1 nm to 160 um: Quantitative estimates for planetary studies. *Astrophys. J.* **757**, 1–12. https://doi.org/10.1088/0004-637X/757/1/95.

Coltice N., Marty B. and Yokochi R. (2009) Xenon isotope constraints on the thermal evolution of the early Earth. *Chem. Geol.* **266**, 4–9. https://doi.org/10.1016/j.chemgeo.2009.04.017.

Conrad P. G., Malespin C. A., Franz H. B., Pepin R. O., Trainer M. G., Schwenzer S. P., Atreya S. K., Freissinet C., Jones J. H., Manning H., Owen T., Pavlov A. A., Wiens R. C., Wong M. H. and Mahaffy P. R. (2016) In situ measurement of atmospheric krypton and xenon on Mars with Mars Science Laboratory. *Earth Planet. Sci. Lett* **454**, 1–9. https://doi.org/10.1016/j.epsl.2016.08.028.

Dauphas N. (2003) The dual origin of the terrestrial atmosphere. *Icarus* **165**, 326–339. https://doi.org/10.1016/S0019-1035(03)00198-2.

Dauphas N. and Morbidelli A. (2014) Geochemical and Planetary Dynamical Views on the Origin of Earth's Atmosphere and Oceans. In Treatise on Geochemistry (Second Edition) (ed. H. D. H. K. Turekian). Treatise on Geochemistry (Second Edition). Elsevier, Oxford. pp. 1–35. https://doi.org/10.1016/B978-0-08-095975-7.01301-2.

Davis D. W., Pezzutto F. and Ojakangas R. W. (1990) The age and provenance of metasedimentary rocks in the Quetico Subprovince, Ontario, from single zircon analyses: implications for Archean sedimentation and tectonics in the Superior Province. *Earth Planet. Sci. Lett* **99**, 195–205. https://doi.org/10.1016/0012-821X(90)90110-J.

de Ronde C. E. J. and Wit M. J. (1994) Tectonic history of the Barberton greenstone belt, South Africa: 490 million years of Archean crustal evolution. *Tectonics* **13**, 983–1005. https://doi.org/10.1029/94TC00353.

Drescher J., Kirsten T. and Schäfer K. (1998) The rare gas inventory of the continental crust, recovered by the KTB Continental Deep Drilling Project. *Earth Planet. Sci. Lett* **154**, 247–263. https://doi.org/10.1016/S0012-821X(97)00185-4.

Farquhar J. and Wing B. A. (2003) Multiple sulfur isotopes and the evolution of the atmosphere. *Earth Planet. Sci. Lett* **213**, 1–13. https://doi.org/10.1016/S0012-821X(03)00296-6.

Foriel J., Philippot P., Rey P., Somogyi A., Banks D. and Ménez B. (2004) Biological control of Cl/Br and low sulfate concentration in a 3.5-Gyr-old seawater from North Pole, Western Australia. *Earth Planet. Sci. Lett.* **228**, 451–463. https://doi.org/10.1016/j.epsl.2004.09.034.

Formisano V., Atreya S., Encrenaz T., Ignatiev N. and Giuranna M. (2004) Detection of methane in the atmosphere of Mars. *Science* **306**, 1758–1761. https://doi.org/10.1126/science.1101732.

Frick U., Mack R., Chang S. (1977) Noble gas trapping and fractionation during synthesis of carbonaceous matter. In Lunar and Planetary Science Conference, 10th, Houston, Tex., March 19–23, 1979, Proceedings. Volume 2. (A80-23617 08-91) New York, Pergamon Press, Inc., 1979, pp. 1961–1972.

Giuliani G., Silva L. J. H. D. and Couto P. (1990) Origin of emerald deposits of Brazil. *Mineral. Deposita* **25**, 57–64. https://doi.org/10.1007/BF03326384.

Giuliani G., France-Lanord C., Cheilletz A., Coget P., Branquet Y. and Laumomnier B. (2000) Sulfate reduction by organic matter in Colombian emerald deposits: chemical and stable isotope (C, O, H) evidence. *Econ. Geol.* **95**, 1129–1153. https://doi.org/10.2113/95.5.1129.

Goldblatt C., Claire M. W., Lenton T. M., Matthews A. J., Watson A. J. and Zahnle K. J. (2009) Nitrogen-enhanced greenhouse warming on early Earth. *Nat. Geosci.* **2**, 891–896. https://doi.org/10.1038/ngeo692.

Havig J. R., Hamilton T. L., Bachan A. and Kump L. R. (2017) Sulfur and carbon isotopic evidence for metabolic pathway evolution and a four-stepped Earth system progression across the Archean and Paleoproterozoic. *Earth Sci. Rev.* **74**, 1–21. https://doi.org/10.1016/j.earscirev.2017.06.014.

Hébrard E. and Marty B. (2014) Coupled noble gas-hydrocarbon evolution of the early Earth atmosphere upon solar UV irradiation. *Earth Planet. Sci. Lett.* **385**, 40–48. https://doi.org/10.1016/j.epsl.2013.10.022.

Holland G. and Ballentine C. J. (2006) Seawater subduction controls the heavy noble gas composition of the mantle. *Nature* **441**, 186–191. https://doi.org/10.1038/nature04761.

Holland G., Cassidy M. and Ballentine C. J. (2009) Meteorite Kr in Earth's mantle suggests a late accretionary source for the atmosphere. *Science* **326**(5959), 1522–1525. https://doi.org/10.1126/science.1179518.

Holland G., Lollar B. S., Li L., Lacrampe-Couloume G., Slater G. F. and Ballentine C. J. (2013) Deep fracture fluids isolated in the crust since the Precambrian era. *Nature* **497**, 357–360. https://doi.org/10.1038/nature12127.

Hunten D. M., Pepin R. O. and Walker J. C. (1987) Mass fractionation in hydrodynamic escape. *Icarus* **69**, 532–549. https://doi.org/10.1016/0019-1035(87)90022-4.

Johnston D. T. (2011) Multiple sulfur isotopes and the evolution of Earth's surface sulfur cycle. *Earth Sci. Rev.* **106**, 161–183. https://doi.org/10.1016/j.earscirev.2011.02.003.

Kendrick M. A., Burgess R., Pattrick R. A. D. and Turner G. (2001) Halogen and Ar–Ar age determinations of inclusions within quartz veins from porphyry copper deposits using complementary noble gas extraction techniques. *Chem. Geol.* **177**, 351–370. https://doi.org/10.1016/S0009-2541(00)00419-8.

Kennedy B. M., Hiyagon H. and Reynolds J. H. (1990) Crustal neon: a striking uniformity. *Earth Planet. Sci. Lett.* **98**, 277–286. https://doi.org/10.1016/0012-821X(90)90030-2.

Kuga M., Cernogora G., Marrocchi Y., Tissandier L. and Marty B. (2017) Processes of noble gas elemental and isotopic fractionations in plasma-produced organic solids: cosmochemical implications. *Geochim. Cosmochim. Acta* **217**, 219–230. https://doi.org/10.1016/j.gca.2017.08.031.

Kuga M., Marty B., Marrocchi Y. and Tissandier L. (2015) Synthesis of refractory organic matter in the ionized gas phase of the solar nebula. *Proc. Natl. Acad. Sci.* **112**, 7129–7134. https://doi.org/10.1073/pnas.1502796112.

Kulikov V. S., Bychkova Y. V., Kulikova V. and Ernst R. (2010) The Vetreny Poyas (Windy Belt) subprovince of southeastern Fennoscandia: an essential component of the ca. 2.5-2.4Ga Sumian large igneous provinces. *Precambr. Res.* **183**, 589–601. https://doi.org/10.1016/j.precamres.2010.07.011.

Kyser K., Hiatt E., Renac C., Durocher K., Holk G. and Deckart K. (2000) Diagenetic fluids in Paleo-and Meso-Proterozoic sedimentary basins and their implications for long protracted fluid histories. In Fluids and basin evolution (ed. K. Kyser). Fluids and basin evolution. pp. 73–506.

Le Mignot E., Siebenaller L., Béziat D., Salvi S., André-Mayer A. S., Reisberg L., Velasquez G., Zimmermann C. and Franceschi G. (2014) The paleoproterozoic copper-gold deposit of Gaoua, Burkina Faso: evidence for a polyphased mineralization. *Acta Geol. Sin. (English Edition)* **88**, 970–972.

Lee J.-Y., Marti K., Severinghaus J. P., Kawamura K., Yoo H.-S., Lee J. B. and Kim J. S. (2006) A redetermination of the isotopic abundances of atmospheric Ar. *Geochim. Cosmochim. Acta* **70**, 4507–4512. https://doi.org/10.1016/j.gca.2006.06.1563.

Lichtenegger H. I. M., Lammer H., Grießmeier J. M., Kulikov Y. N., Paris von P., Hausleitner W., Krauss S. and Rauer H. (2010) Aeronomical evidence for higher CO_2 levels during Earth's Hadean epoch. *Icarus* **210**, 1–7. https://doi.org/10.1016/j.icarus.2010.06.042.

Lippmann-Pipke J., Lollar B. S., Niedermann S., Stroncik N. A., Naumann R., van Heerden E. and Onstott T. C. (2011) Neon identifies two billion year old fluid component in Kaapvaal Craton. *Chem. Geol.* **283**, 287–296. https://doi.org/10.1016/j.chemgeo.2011.01.028.

Lyons T. W., Reinhard C. T. and Planavsky N. J. (2014) The rise of oxygen in Earth's early ocean and atmosphere. *Nature* **506**, 307–315. https://doi.org/10.1038/nature13068.

Mark D. F., Rice C. M., Fallick A. E., Trewin N. H., Lee M. R., Boyce A. and Lee J. K. W. (2011) $^{40}Ar/^{39}Ar$ dating of hydrothermal activity, biota and gold mineralization in the Rhynie hot-spring system, Aberdeenshire, Scotland. *Geochim. Cosmochim. Acta* **75**, 555–569. https://doi.org/10.1016/j.gca.2010.10.014.

Marrocchi Y., Marty B., Reinhardt P. and Robert F. (2011) Adsorption of xenon ions onto defects in organic surfaces: implications for the origin and the nature of organics in

primitive meteorites. *Geochim. Cosmochim. Acta* **75**, 6255–6266. https://doi.org/10.1016/j.gca.2011.07.048.

Marty B. (2012) The origins and concentrations of water, carbon, nitrogen and noble gases on Earth. *Earth Planet. Sci. Lett.* **313–314**, 56–66. https://doi.org/10.1016/j.epsl.2011.10.040.

Marty B. and Zimmermann L. (1999) Volatiles (He, C, N, Ar) in mid-ocean ridge basalts: assessment of shallow-level fractionation and characterization of source composition. *Geochim. Cosmochim. Acta* **63**, 3619–3633. https://doi.org/10.1016/S0016-7037(99)00169-6.

Marty B., Altwegg K., Balsiger H., Bar-Nun A., Bekaert D. V., Berthelier J. J., Bieler A., Briois C., Calmonte U., Combi M., De Keyser J., Fiethe B., Fuselier S. A., Gasc S., Gombosi T. I., Hansen K. C., Hässig M., Jackel A., Kopp E., Korth A., Le Roy L., Mall U., Mousis O., Owen T., Reme H., Rubin M., Semon T., Tzou C. Y., Waite J. H. and Wurz P. (2017) Xenon isotopes in 67P/Churyumov-Gerasimenko show that comets contributed to Earth's atmosphere. *Science* **356**, 1069–1072. https://doi.org/10.1126/science.aal3496.

Marty B., Zimmermann L., Pujol M., Burgess R. and Philippot P. (2013) Nitrogen isotopic composition and density of the Archean atmosphere. *Science* **342**, 101–104. https://doi.org/10.1126/science.1240971.

Marty B., Avice G., Sano Y., Altwegg K., Balsiger H., Hässig M., Morbidelli A., Mousis O. and Rubin M. (2016) Origins of volatile elements (H, C, N, noble gases) on Earth and Mars in light of recent results from the ROSETTA cometary mission. *Earth Planet. Sci. Lett.* **441**, 91–102. https://doi.org/10.1016/j.epsl.2016.02.031.

Marty B., Avice G., Bekaert D. V., Broadley M. W. (2018) Salinity of the Archean oceans from analysis of fluid inclusions in quartz. CR Geosci., in press. https://doi.org/10.1016/j.crte.2017.12.002.

Meshik A. P., Hohenberg C. M., Pravdivtseva O. V. and Kapusta Y. S. (2001) Weak decay of 130Ba and 132Ba: geochemical measurements. *Phys. Rev. C* **64**, 035205. https://doi.org/10.1103/PhysRevC.64.035205.

Mezhelovskaya S. V., Korsakov A. K., Mezhelovskii A. D. and Bibikova E. V. (2016) Age range of formation of sedimentary volcanogenic complex of the vetreny belt (the Southeast of the Baltic Shield). *Petrology* **24**, 105–117. https://doi.org/10.1134/S0869593816020040.

Mukhopadhyay S. (2012) Early differentiation and volatile accretion recorded in deep-mantle neon and xenon. *Nature* **486**, 101–104. https://doi.org/10.1038/nature11141.

Nisbet E. G. and Sleep N. (2001) The habitat and nature of early life. *Nature* **409**, 1083–1091.

Nutman A. P. and Friend C. R. L. (2009) New 1:20,000 scale geological maps, synthesis and history of investigation of the Isua supracrustal belt and adjacent orthogneisses, southern West Greenland: a glimpse of Eoarchaean crust formation and orogeny. *Precambr. Res.* **172**, 189–211. https://doi.org/10.1016/j.precamres.2009.03.017.

Ott U. (1988) Noble gases in SNC meteorites: Shergotty, Nakhla, Chassigny. *Geochim. Cosmochim. Acta* **52**(7), 1937–1948. https://doi.org/10.1016/0016-7037(88)90017-8.

Ott U. (2014) Planetary and pre-solar noble gases in meteorites. *Chem. Erde* **74**, 519–544. https://doi.org/10.1016/j.chemer.2014.01.003.

Ozima M. and Nakazawa K. (1980) Origin of rare gases in the Earth. *Nature* **284**, 313–316. https://doi.org/10.1038/284313a0.

Ozima M. and Podosek F. A. (2002) *Noble Gas Geochemistry*, second ed. Cambridge University Press, Cambridge.

Parai R. and Mukhopadhyay S. (2015) The evolution of MORB and plume mantle volatile budgets: constraints from fission Xe isotopes in Southwest Indian Ridge basalts. *Geochem. Geophys.* **16**, 1–17. https://doi.org/10.1002/2014GC005566.

Pavlov A. A. and Kasting J. F. (2002) Mass-independent fractionation of sulfur isotopes in Archean sediments: strong evidence for an anoxic Archean atmosphere. *Astrobiology* **2**, 27–41. https://doi.org/10.1089/153110702753621321.

Pepin R. O. (2013) Comment on "Chondritic-like xenon trapped in Archean rocks: a possible signature of the ancient atmosphere" by M. Pujol, B. Marty, R. Burgess [Earth Planet. Sci. Lett. 308 (2011) 298–306]. *Earth Planet. Sci. Lett.* **371–372**, 294–295. https://doi.org/10.1016/j.epsl.2013.03.027.

Pepin R. O. (1991) On the origin and early evolution of terrestrial planet atmospheres and meteoritic volatiles. *Icarus* **92**, 2–79. https://doi.org/10.1016/0019-1035(91)90036-S.

Péron S., Moreira M., Putlitz B. and Kurz M. D. (2017) Solar wind implantation supplied light volatiles during the first stage of Earth accretion. *Geochem. Persp. Let.* **3**, 151–159. https://doi.org/10.7185/geochemlet.1718.

Philippot P., van Zuilen M. and Rollion-Bard C. (2012) Variations in atmospheric sulphur chemistry on early Earth linked to volcanic activity. *Nat. Geosci.* **5**, 668–674. https://doi.org/10.1038/ngeo1534.

Planavsky N. J., Asael D., Hofmann A., Reinhard C. T., Lalonde S. V., Knudsen A., Wang X., Ossa Ossa F., Pecoits E., Smith A. J. B., Beukes N. J., Bekker A., Johnson T. M., Konhauser K. O., Lyons T. W. and Rouxel O. J. (2014) Evidence for oxygenic photosynthesis half a billion years before the Great Oxidation Event. *Nat. Geosci.* **7**, 283–286. https://doi.org/10.1038/ngeo2122.

Puchtel I. S., Haase K. M., Hofmann A. W., Chauvel C., Kulikov V. S., Garbe-Schonberg C. D. and Nemchin A. A. (1997) Petrology and geochemistry of crustally contaminated komatiitic basalts from the Vetreny Belt, southeastern Baltic Shield: evidence for an early Proterozoic mantle plume beneath rifted Archean continental lithosphere. *Geochim. Cosmochim. Acta* **61**, 1205–1222. https://doi.org/10.1016/S0016-7037(96)00410-3.

Puchtel I. S., Touboul M., Blichert-toft J., Walker R. J., Brandon A. D., Nicklas R. W., Kulikov V. S. and Samsonov A. V. (2016) Lithophile and siderophile element systematics of Earth ' s mantle at the Archean – proterozoic boundary: evidence from 2.4 Ga komatiites. *Geochim. Cosmochim. Acta* **180**, 227–255. https://doi.org/10.1016/j.gca.2016.02.027.

Pujol M., Marty B. and Burgess R. (2011) Chondritic-like xenon trapped in Archean rocks: a possible signature of the ancient atmosphere. *Earth Planet. Sci. Lett.* **308**, 298–306. https://doi.org/10.1016/j.epsl.2011.05.053.

Pujol M., Marty B., Burgess R., Turner G. and Philippot P. (2013a) Argon isotopic composition of Archaean atmosphere probes early Earth geodynamics. *Nature* **498**, 87–90. https://doi.org/10.1038/nature12152.

Pujol M., Marty B. and Burgess R. (2013b) Reply to comment on "Chondritic-like xenon trapped in Archean rocks: a possible signature of the ancient atmosphere" by Pujol, M., Marty, B., Burgess, R., Earth and Planetary Science Letters 308 (2011) 298–306 by Pepin, R. O.. *Earth Planet. Sci. Lett.* **371–372**, 296–298. https://doi.org/10.1016/j.epsl.2013.03.029.

Pujol M., Marty B., Burnard P. and Philippot P. (2009) Xenon in Archean barite: weak decay of 130Ba, mass-dependent isotopic fractionation and implication for barite formation. *Geochim. Cosmochim. Acta* **73**, 6834–6846. https://doi.org/10.1016/j.gca.2009.08.002.

Ramirez R. M. (2013) Warming early Mars with CO_2 and H_2. *Nat. Geosci.* **7**, 59–63. https://doi.org/10.1038/ngeo2000.

Reimold W. U. and Koeberl C. (2014) Impact structures in Africa: a review. *J. Afr. Earth Sci.* **93**, 57–175. https://doi.org/10.1016/j.jafrearsci.2014.01.008.

Ribas I., Guinan E. F., Gudel M. and Audard M. (2005) Evolution of the solar activity over time and effects on planetary atmospheres. I. High-energy irradiances (1–1700 Å). *Astrophys. J.* **622**, 680–694. https://doi.org/10.1086/427977.

Rice C. M., Ashcroft W. A., Batten D. J., Boyce A. J., Caulfield J. B. D., Fallick A. E., Hole M. J., Jones E., Pearson M. J., Rogers G., Saxton J. M., Stuart F. M., Trewin N. H. and Turner G. (1995) A Devonian auriferous hot spring system, Rhynie, Scotland.. *J. Geol. Soc. London* **152**, 229–250. https://doi.org/10.1144/gsjgs.152.2.0229.

Rose N. M., Rosing M. T. and Bridgwater D. (1996) The origin of metacarbonate rocks in the Archaean Isua supracrustal belt, West Greenland. *Am. J. Sci.* **296**, 1004–1044. https://doi.org/10.2475/ajs.296.9.1004.

Schwarzschild M. (1958) Structure and Evolution of the Stars. Princeton University Press, Dover Publications Inc., Princeton.

Srinivasan B. (1976) Barites: anomalous xenon from spallation and neutron-induced reactions. *Earth Planet. Sci. Lett.* **31**, 129–141. https://doi.org/10.1016/0012-821X(76)90104-7.

Srinivasan B., Alexander E. C., Jr and Manuel O. K. (1971) Iodine-129 in terrestrial ores. *Science* **173**, 327–328. https://doi.org/10.1126/science.173.3994.327.

Stuart F. M., Mark D. F., Gandanger P. and McConville P. (2016) Earth-atmosphere evolution based on new determination of Devonian atmosphere Ar isotopic composition. *Earth Planet. Sci. Lett.* **446**, 21–26. https://doi.org/10.1016/j.epsl.2016.04.012.

Takaoka N. (1972) An interpretation of general anomalies of xenon and the isotopic composition of primitive xenon. *Mass Spec.* **20**, 287–302. https://doi.org/10.5702/massspec1953.20.287.

Tarduno J. A., Blackman E. G. and Mamajek E. E. (2014) Detecting the oldest geodynamo and attendant shielding from the solar wind: Implications for habitability. *Phys. Earth Planet. Inter.* **233**, 68–87. https://doi.org/10.1016/j.pepi.2014.05.007.

Trendall A. F., Compston W., Nelson D. R., De Laeter J. R. and Bennett V. C. (2004) SHRIMP zircon ages constraining the depositional chronology of the Hamersley Group, Western Australia. *Aust. J. Earth Sci.* **51**, 621–644. https://doi.org/10.1111/j.1400-0952.2004.01082.x.

Ulrich R. K. (1975) Solar neutrinos and variations in the solar luminosity. *Science* **190**, 619–624.

Warr O., Sherwood Lollar B., Fellowes J., Sutcliffe C. N., McDermott J. M., Holland G., Mabry J. C. and Ballentine C. J. (2018) Tracing ancient hydrogeological fracture network age and compartmentalisation using noble gases. *Geochim. Cosmochim. Acta* **222**, 340–362. https://doi.org/10.1016/j.gca.2017.10.022.

Yokochi R. and Marty B. (2004) A determination of the neon isotopic composition of the deep mantle. *Earth Planet. Sci. Lett.* **225**, 77–88. https://doi.org/10.1016/j.epsl.2004.06.010.

Zahnle K. J. (2015) Xenon Fractionation and Archean Hydrogen Escape. In 46th Lunar and Planetary Science Conference. The Woodlands (Texas). Abstracts #1549.

Zahnle K. J. (2018) Xenon fractionation and Archean hydrogen escape. II. Now More Than Ever. In 49th Lunar and Planetary Science Conference. The Woodlands (Texas) Abstract #2536.

Zahnle K. J. and Kasting J. F. (1986) Mass fractionation during transonic escape and implications for loss of water from Mars and Venus. *Icarus* **68**, 462–480. https://doi.org/10.1016/0019-1035(86)90051-5.

Zahnle K. J., Pollack J. B. and Kasting J. F. (1993) Xenon fractionation in porous planetesimals. *Geochim. Cosmochim. Acta* **54**, 2577–2586. https://doi.org/10.1016/0016-7037(90)90243-E.

Zahnle K. J., Catling D. C. and Claire M. W. (2013) The rise of oxygen and the hydrogen hourglass. *Chem. Geol.* **362**, 26–34. https://doi.org/10.1016/j.chemgeo.2013.08.004.

Zakharov D. and Bindeman I. N. (2015) Stable Isotope Geochemistry of Extremely Well-Preserved 2.45-Billion-Year-Old Hydrothermal Systems in the Vetreny Belt, Baltic Shield: Insights into Paleohydrosphere. In 2015 AGU Fall Meeting Abstracts #PP33B-2297.

Zimmermann L. (2014) Méthode d'extraction des gaz rares sous ultravide. *Techniques de l'ingénieur* **J6632**, 1–21.

Zimmermann L., Avice G., Blard P.-H., Marty B., Füri E. and Burnard P. G. (2017) A new all-metal induction furnace for noble gas extraction. *Chem. Geol.* **480**, 86–92. https://doi.org/10.1016/j.chemgeo.2017.09.018.

Associate Editor: Nicolas Dauphas